THz Propagation of Surface Plasmon Polariton in Ag-InP Interface

by

Ta-Seen Haque Dhrubo (ID-142413)
Shadman Raihan (ID-142419)
Asif Newaz (ID-142427)

A Thesis Submitted to the Academic Faculty in Partial Fulfillment of the Requirements for the Degree of

BACHELOR OF SCIENCE IN ELECTRICAL AND ELECTRONIC ENGINEERING

Department of Electrical and Electronic Engineering
Islamic University of Technology (IUT)
Gazipur, Bangladesh

November 2018

THz Propagation of Surface Plasmon Polariton in Ag-InP Interface

Approved by:

Dr. Rakibul Hasan Sagor

Supervisor and Assistant Professor,
Department of Electrical and Electronic Engineering,
Islamic University of Technology (IUT),
Boardbazar, Gazipur-1704.

Date:

Table of Contents

List of Tables

List of Figures

Acknowledgements

We would like to convey our sincere gratitude to our advisor Prof. Dr. Rakibul Hasan Sagor for the continuous guidance for our thesis and related research, for his patience, motivation, and immense knowledge. Without his depth of knowledge and thoughts our thesis work would be severely lacking. His supervision helped us all the time of research and writing of this thesis. We could not have imagined having a better advisor and mentor for our thesis.

Abstract

The existence of surface plasmon polaritons was first predicted in 1957 by Rufus Ritchie. But at that time its application was unknown. The 2nd birth of SPPs occurred after 1997 when scientists realized that it can be used localize the light signals far beyond the diffraction limit; the limit which is the main hindrance in integration and miniaturization of optical devices. Following the discovery, research in this field has been growing rapidly. SPPs are basically electromagnetic waves which arise from the coupling effect between photons and the free conduction electrons on the interface between a metal and a dielectric. They propagate along the interface. In this thesis, propagation characteristics of Surface Plasmon Polaritons in the single interface of Silver (Ag) and Indium Phosphide (InP) are presented. A three dimensional structure has been designed to analyze the dynamics of the propagation numerically. Lorentz-Drude model is used to model the frequency dependent permittivity of Ag while Lorentz model is used to model InP. The dimensions of Indium Phosphide layer are varied to find an optimum design which grants the highest efficiency. The nano-plasmonic structure yields an efficiency of 59.76%.

Chapter 1

Introduction

In recent years, plasmonics has become a very attractive field of research due to its potential applications in numerous sectors. It allows the concentration of light into regions as small as few nanometers which was not possible before due to the diffraction limit of optical modes [1]. This property is utilized in developing superlenses [2], hyperlenses [3], control switches and modulators [4] [5], bragg reflectors [6] etc. Enhanced propagation of SPPs can help in the miniaturization of photonic ICs. The ability to excite EM waves on a sub-wavelength scale is used in THz applications such as sensors, biological spectroscopy, non-destructive spectroscopy, optical antennas, high-frequency communication, cathodo-luminescence and many others [7][8]. Research in this area is likely to bring forth many other prospective applications in the near future.

1.1 General overview:

Surface plasmon polaritons are excited upon the application of LASER light in the interface between a metal and a dielectric. Metal provides abundant free electrons in the conduction band. The incident light excites the electrons on the surface of the metal which causes electron oscillation. A plasmon is a quantum of plasma oscillation. Just as light (an optical oscillation) consists of photons, the plasma oscillation consists of plasmons. They are the collective oscillations of the free electrons. When plasmons and photon are coupled together, the resulting hybridized excitation is called Surface Plasmon-Polariton (SPP).

SPPs propagate along the interface of the metal and dielectric until it loses its' energy either due to absorption in the metal or scattering into other directions. This propagation loss limits the possibility of many applications. It cannot be eliminated but can be minimized. Enhanced propagation can be a pioneering step in the miniaturization of photonic devices.

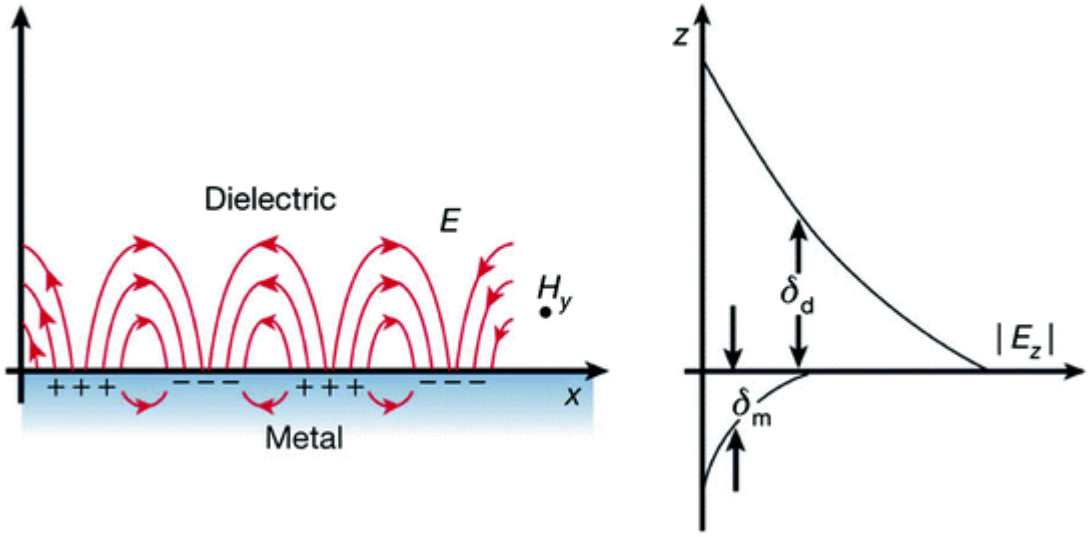

Figure 1.1: Surface Plasmon-polaritons propagation at the interface of metal a dielectric.

1.2 Nanoplasmonic coupler

Different metal dielectric structures provide different propagation characteristics. At [9] Ghulam Saber presented a nanoplasmonic coupler which provides 67% efficiency. F Lou demonstrated an ultra-compact directional coupler in [10]. In our thesis we've worked with a nanoplasmonic structure which provides 59.76% efficiency. The schematic diagram of the structure is shown in figure-1.2.

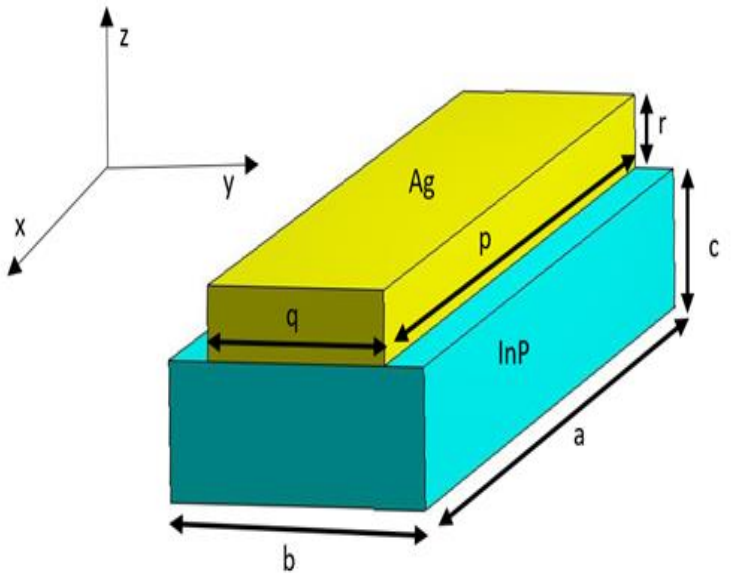

Figure 1.2: Schematic diagram of the nanoplasmonic structure

The three-dimensional model of the proposed structure has been developed in CST where time domain solver was used for the simulation purpose. The width and height of the InP layer was varied one at a time. At different width, the efficiency of the coupler was determined. Then again at different height, the efficiency of the coupler was determined. This way the optimum dimension was measured for which the coupler provides maximum efficiency. The reflection coefficient, return loss, VSWR, transmission coefficient and insertion loss was determined for the structure having the highest efficiency to evaluate the performance of SPP propagation.

1.3 Numerical methods

SPPs are electromagnetic excitations. Their propagation is described by Maxwell's equations. The experimental approach for any electromagnetic

analysis needs a lot of efforts, cost and time. It is not economically viable to go for a particular experimental research by changing different parameters of the experimental setup, especially when the apparatus are very costly to manufacture. That is why simulation is becoming popular to most of the researchers, which gives almost exact output, if the system is modeled perfectly. This does not mean that experiments are not needed. It only means that accurate system simulation results fewer and more efficient experiments and thus results in important savings in costs and effort.

There are two main approaches to evaluate electromagnetic quantities:

1. Analytical method
2. Numerical method

The most used analytical methods are:

1. Separation of variables
2. Series Expansion
3. Perturbation

The analytical approaches may fail when the solution region is complex, the Partial Differential Equations (PDE) are not linear, or if there are time dependent boundary conditions. So to overcome these problems, numerical techniques are being used.

There are various numerical methods which are currently being used by different researchers. Some well-known techniques are:

1. Finite Difference Time Domain (FDTD) method
2. Method of Line (MOL)
3. Beam Propagation Method (BPM)
4. Finite Element Method (MEM)

5. Transmission-line-matrix Method
6. Monte Carlo Methods etc.

The research work which is reported in this thesis is mainly based on the FDTD method. But the work can be simulated using other methods as well.

1.4 Finite Difference Time Domain (FDTD) method

FDTD method is one of the most widely used methods in computational electromagnetics. The FDTD algorithm was first introduced by Yee in 1966[11] where he described the basis of the first space-grid time domain technique for Maxwell's curl equation. Without requiring a complex mathematical formulation, it provides us with a simple way to discretize Maxwell's equations and it does not need any symmetry in the structure being modeled. Moreover, it computes the solution in the time domain, from which the frequency behavior can be extracted over a wide range of frequencies. Since the introduction of the FDTD algorithm, it has undergone many modifications. This method is gaining more popularity and a lot of FDTD-related research activities are being done. It is more accurate and robust and is likely remain one of the dominant computational electrodynamics techniques.

1.5 Thesis Objectives

The main objective of this thesis is to analyze the dynamics of the SPP propagation in the interface of Silver and InP numerically. Some other objectives are –

1. To study the properties of propagation of Surface Plasmon Polariton in different media.
2. To compare between different dielectric materials which provides higher efficiency.
3. To determine the optimum dimension for which highest efficiency is obtained.
4. To develop a simulator capable of presenting the propagation dynamics of SPP.
5. Using the simulator, carry out studies on SPP propagation.

Chapter 2

Surface Plasmon Polaritons

2.1 Overview

A plasmon is a quantum of plasma oscillation. Just as light, an optical oscillation, consists of photons, the plasma oscillation consists of plasmons. Polaritons are hybrid particles or quasiparticle made up of a photon strongly coupled to an electric dipole. When the photon is coupled with oscillating electrons at the surface of a metal, surface-plasmon polaritons are geenrated.

When a light beam is incident on a metal in a certain way, the electrons on the metal surface gets excited and starts to oscillate. But SPPs cannot be directly excited by light beams; prism coupling or grating coupling is required to provide enough momentum to excite SPP. Once they are generated, they propagate along metal- dielectric interface.

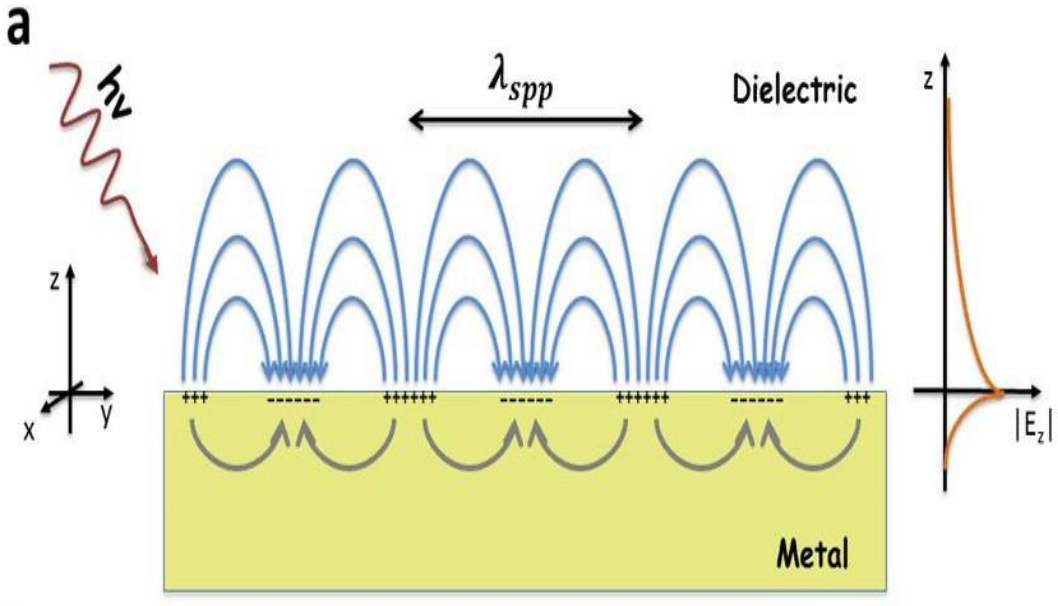

Figure 2.1: Surface Plasmon polaritons propagation at the interface of metal and dielectric.

The term ‘surface plasmon polariton’ means that the wave involves both charge motion in the metal (‘surface plasmon’) and electromagnetic waves in the air or dielectric (‘polariton’). They are a type of surface wave, guided along the interface in much the same way that light can be guided by an optical fiber. SPPs are shorter in wavelength than the incident light (photons). Hence, SPPs can have tighter spatial confinement and higher local field intensity. Perpendicular to the interface, they have subwavelength-scale confinement. An SPP will propagate along the interface until its energy is lost either due to absorption in the metal or scattering into other directions.

2.2 SPP Propagation

Surface Plasmon Polaritons are electromagnetic waves propagating along the interface between a dielectric and a conductor, confined in the perpendicular direction. Electromagnetic wave propagation is described by Maxwell’s equations. So we need to apply Maxwell’s equations on the interface.

Maxwell’s equations can be described in the following form:

$$\nabla . D = \rho$$
$$\nabla . B = 0$$
$$\nabla \times E = -\frac{\partial B}{\partial t}$$
$$\nabla \times H = J_{ext} + \frac{\partial D}{\partial t}$$

where

E is the electric field vector in volt per meter

D is the electric flux density vector in coulombs per square meter

H is the magnetic field vector in amperes per meter

B is the magnetic flux density vector in Webbers per square meter

ρ is the charge density

J_{ext} is the current density

The electric and magnetic fields are related to polarization P and magnetization M –

$$H = \frac{1}{\mu_0} + B - M$$

`` $$D = \varepsilon_0 E + P$$

For linear, isotropic and nonmagnetic media the relation can be simplified to –

$$D = \varepsilon_0 \varepsilon_r E$$
$$B = \mu_o \mu_r H$$

where

ε_0 is the electric permittivity of vacuum in Farad per meter

μ_o is the magnetic permeability of vacuum in Henry per meter

ε_r is the relative permittivity

μ_r is the relative permeability

The field E and H can be decomposed in Cartesian coordinate system as

$$E = E_x . \overrightarrow{a_x} + E_y . \overrightarrow{a_y} + E_z . \overrightarrow{a_z}$$
$$H = H_x . \overrightarrow{a_x} + H_y . \overrightarrow{a_y} + H_z . \overrightarrow{a_z}$$

For harmonic time dependence, by solving Ampere's law and Faraday's law, the following set of coupled equations can be obtained –

$$\frac{\partial E_Z}{\partial y} - \frac{\partial E_y}{\partial z} = j\omega\mu_0 H_x$$
$$\frac{\partial E_x}{\partial z} - \frac{\partial E_z}{\partial x} = j\omega\mu_0 H_y$$
$$\frac{\partial E_y}{\partial x} - \frac{\partial E_x}{\partial y} = j\omega\mu_0 H_z$$
$$\frac{\partial H_Z}{\partial y} - \frac{\partial H_y}{\partial z} = -j\omega\varepsilon_r E_X$$
$$\frac{\partial H_X}{\partial z} - \frac{\partial H_Z}{\partial x} = -j\omega\varepsilon_r E_Y$$
$$\frac{\partial H_y}{\partial x} - \frac{\partial H_x}{\partial y} = -j\omega\varepsilon_r E_z$$

Since the propagation is assumed along x-direction in the form $e^{j\beta x}$, it then follows that $\frac{\partial}{\partial x} = -j\beta.$

The homogeneity in the y-direction results in $\frac{\partial}{\partial y} = 0.$ So the equations can be simplified to --

$$-\frac{\partial E_y}{\partial z} = j\omega\mu_0 H_x$$
$$\frac{\partial E_x}{\partial z} - j\beta\, E_z = j\omega\mu_0 H_y$$
$$j\beta \mathrm{E}_\psi = j\omega\mu_0 H_z$$
$$\frac{\partial H_y}{\partial z} = -j\omega\varepsilon_r E_X$$
$$\frac{\partial H_X}{\partial z} - j\beta \mathrm{H}_z = -j\omega\varepsilon_r E_Y$$
$$j\beta \mathrm{H}_y = -j\omega\varepsilon_r E_z$$

There are two sets of independent solutions with different polarization properties: Transverse magnetic (TM) modes and Transverse electric (TE) modes. For the TM modes, the governing equations are –

$$E_x = -j\,\frac{1}{\omega\varepsilon_o\varepsilon}\frac{\partial H_y}{\partial z}$$

$$E_z = -\,\frac{\beta}{\omega\varepsilon_o\varepsilon}H_y$$

The wave equation for TM polarized wave becomes

$$\frac{\partial^2 H_y}{\partial z^2} + (k_o^2\varepsilon - \beta^2)H_y = 0$$

Similarly, for TE polarized the equation sets are

$$H_x = j\,\frac{1}{\omega\mu_o}\frac{\partial E_y}{\partial z}$$

$$H_z = \frac{\beta}{\omega\mu_o}E_y$$

The wave equation for TE waves becomes

$$\frac{\partial^2 E_y}{\partial z^2} + (k_o^2\varepsilon - \beta^2)E_y = 0$$

There are no surface modes for the TE polarization. SPPs exist only for the TM polarization.

Chapter 3

Choice of Material

Surface Plasmon Polaritons propagate on the surface of the metal. The major obstacle in that is the loss associated with it which limits the propagation length of the SPPs. It also broadens the bandwidth of resonances. The loss is mainly dissipative loss which occurs due to the conversion of optical energy to heat. At higher frequencies (in THz range), the loss also increases. So finding a suitable material for enhanced SPP propagation is necessary. At [9] Ghulam Saber demonstrated Gallium Lanthanum Sulfide based coupler with 67% efficiency. At [12] Gururaj V. Naik represented different alternative materials for plasmonic operations.

InP has been used in this research as the dielectric material. It is a direct bandgap semiconductor and one of the most widely used materials in optoelectronic applications. It provides the advantages like easy integration and compatibility with conventional optoelectronic devices and their fabrication. It is generally used for telecom applications at 1300nm and 1550nm wavelengths. At [13], M.E.Panah used InP for application in mid-IR region. However, for wavelength of 300-800nm, to the extent of our knowledge, this is the first time one has performed a detailed investigation of SPP propagation.

In case of metal, one with the lowest loss would be the appropriate choice for plasmonic applications. Silver (Ag) has been used in this research. Silver and gold are the best materials for applications in visible and near infrared light range. There are many loss mechanism that limit a materials usefulness for plasmonic applications. The most influential are energy loss from intraband transitions and ohmic loss caused by electron-electron scattering, electron-ion scattering, and

inelastic scattering from defects and grain boundaries. These losses are material dependent and wavelength dependent.

The table below shows the dampening and the onset of intraband transitions for four of the most commonly used plasmonic materials.

Table 3.1: dampening and the onset of intraband transitions for four of the most commonly used plasmonic materials

Material	Dampening Rate (eV)	Onset of Intraband Transitions (eV)
Silver	0.02	3.9
Gold	0.07	2.3
Coppper	0.07	2.1
Aluminum	0.13	1.41

When choosing a material, it is best to pick the one with the least amount of ohmic loss, and therefore the smallest dampening rate. From the table it is found that silver is the best in this regard. Besides that, Ag also has highest onset of intraband transitions, higher than the energy of the plasmons, which is expectable.

Chapter 4

Material Modelling

At low frequency, metals behave as perfect conductors. But at high frequency, they show dispersion. This behavior causes the existence of fields inside the metal at high frequency. When a material is excited by an electromagnetic field, its permittivity varies with the frequency of the applied field. Material dispersion is defined as the dependence of the dielectric function of a material on the frequency and signifies that a particular material will have different values of its dielectric function as the frequency changes.

The behavior of any material under the application of an electromagnetic field can be determined from three vectors:

Electrical flux density (D)

Electric field intensity (E)

Polarization density (P).

In frequency domain, the relation between them is as follows:

$$D(\omega) = \varepsilon(\omega)E(\omega)$$

$$P(\omega) = \varepsilon_o\chi(\omega)E(\omega)$$

$$D(\omega) = \varepsilon_o E(\omega) + P(\omega)$$

Combining the last two equations, we have –

$$D(\omega) = \varepsilon_o E(\omega)(1 + \chi(\omega)) \qquad (3.4)$$

Here,

χ is the electric susceptibility which is a measure of how easily the dielectric is polarized in response to an applied electric field.

Combining (3.1) and (3.4) we get

$$\varepsilon(\omega) = \varepsilon_o(1 + \chi(\omega))$$

So the relative permittivity can be written as

$$\varepsilon_r(\omega) = 1 + \chi(\omega)$$

The above values become simple for a linear isotropic material. But for a dispersive material, the frequency dependent permittivity and susceptibility are to be modeled perfectly in order to get the perfect response of the material for certain electromagnetic excitation. To model a dispersive material, different models are used. Such as –

1. Drude model
2. Lorentz model
3. Debye model
4. Lorentz-Drude model.

The frequency dependency of the complex dielectric function of a material using the Lorentz oscillator model is given by [14]

$$\varepsilon\,(\omega) = \varepsilon_\infty + \sum_{n=1}^{N_L} \frac{\Delta\varepsilon_n \omega_n^2}{\omega_n^2 + 2j\omega\delta_n - \omega^2}$$

Here,

- ε_∞ -infinite frequency relative permittivity
- N_L - total number of Lorentz pole pairs
- ω_n - n^{th} pole pair undamped frequency
- $\Delta\varepsilon_n$ - change of permittivity of the material for n^{th} pole pair
- δ_n - damping factor.

For InP, 4-pole Lorentz oscillator model has been used. InP is modelled using the parameters that were obtained by R.H. Sagor et al. [15] and this model is valid for wavelength ranging from 250nm to 850nm. Parameters describing the Lorentz oscillator model for InP are shown in table 4.1.

Parameter	Value	Parameter	Value
ε_∞	1.5173	$\delta_3(rad/sec)$	-2.99×10^{14}
$\Delta\varepsilon_1$	4.8703	$\delta_4(rad/sec)$	3.34×10^{14}
$\Delta\varepsilon_2$	1.4047	$\omega_1(rad/sec)$	7.64×10^{15}
$\Delta\varepsilon_3$	1.2563	$\omega_2(rad/sec)$	5.41×10^{15}
$\Delta\varepsilon_4$	1.2096	$\omega_3(rad/sec)$	4.84×10^{15}
$\delta_1(rad/sec)$	-2.1×10^{15}	$\omega_4(rad/sec)$	7.18×10^{15}
$\delta_2(rad/sec)$	-8.14×10^{14}		

Table 4.1: The optimized Lorentz model parameters for InP.

The frequency dependent permittivity of Ag is designed by employing the Lorentz-Drude Six pole model which is represented by [16]

$$\varepsilon_r(w) = 1 - \frac{f_0\omega_P^2}{\omega^2 - j\Gamma_0\omega} + \sum_{i=1}^{5} \frac{f_i\omega_P^2}{\omega_{0i}^2 + j\Gamma_i\omega - \omega^2}$$

Here,

- ω_p - frequency of plasma
- ω_{0i} - pole pair frequency
- f_i - oscillator strength
- Γ_i - frequency of damping

The modelling parameters for Ag are obtained from Rakic et al. [17].

CHAPTER 5

FDTD-BASED SOLUTION

5.1 Introduction to FDTD Method

The theory on the basis of the FDTD method is simple. To solve an electromagnetic problem, the idea is to simply discretize, both in time and space, the Maxwell's equations with central difference approximations. The originality of the idea of Yee resides in the allocation in space of the electric and magnetic field components, and the marching in time for the evolution of the procedure. To better understand the theory of the method, we will start considering a simple one-dimensional problem. Assume, at this stage, "free space" as propagation medium. In this case, Maxwell's equations can be written as

$$\frac{\partial H}{\partial t} = -\frac{1}{\mu}\nabla \times E \qquad 5.1$$

$$\frac{\partial H}{\partial t} = -\frac{1}{\mu}\nabla \times E \qquad 5.2$$

Assuming nonmagnetic media (i.e. $\mu = \mu_0$) expansion of the components of the curl operators of and yields the following six coupled scalar equations in Cartesian coordinates.

$$\frac{\partial E_Z}{\partial y} - \frac{\partial E_y}{\partial z} = j\omega\mu_0 H_x$$

$$\frac{\partial E_x}{\partial z} - \frac{\partial E_z}{\partial x} = j\omega\mu_0 H_y$$

$$\frac{\partial E_y}{\partial x} - \frac{\partial E_x}{\partial y} = j\omega\mu_0 H_z$$

$$\frac{\partial H_Z}{\partial y} - \frac{\partial H_y}{\partial z} = -j\omega\varepsilon_r E_X$$

$$\frac{\partial H_X}{\partial z} - \frac{\partial H_Z}{\partial x} = -j\omega\varepsilon_r E_Y$$

$$\frac{\partial H_y}{\partial x} - \frac{\partial H_x}{\partial y} = -j\omega\varepsilon_r E_z$$

Those partial differential equations form the beginning of the FDTD numerical algorithm for modeling electromagnetic wave interactions with arbitrary three-dimensional objects. The Yee algorithm simultaneously deals with both the electric and magnetic fields in both time and space, rather than by solving the wave equation for either the electric field or the magnetic field alone.

Yee's FDTD scheme discretizes Maxwell's curl equations. It approximates the time and space first-order partial derivatives with central differences, and then solves the resulting equations by using a leapfrog scheme

5.2 Yee's Orthogonal Mesh

Yee proposed a 3-D mesh having field components at different locations as shown in Fig.4.1.1. *E* and *H* components are positioned at the centers of the grid lines and surfaces such that each component is surrounded by four components. This gives a simple picture of three-dimensional space being filled by interlinked arrays of Faraday's law and Ampere's law contours. Thus, it is possible to identify the *E* components related with the displacement current flux linking with the *H* loops and, correspondingly, the *H* components related with the magnetic flux are linked with the E loops, as shown in Fig.5.1.

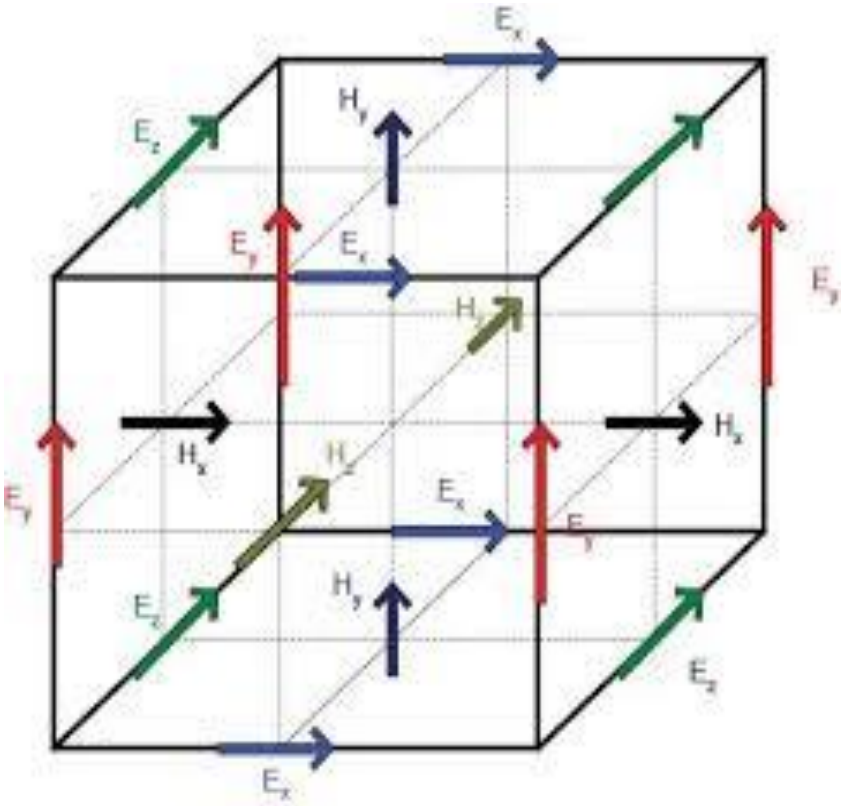

Figure 5.1: Yee's Orthogonal Mesh

If we consider only 2-dimensional space (i.e of x-y plane), and assuming no variation of the fields in the z-direction. Thus we have:

$$\frac{\partial Hy}{\partial z} = 0, \frac{\partial Hx}{\partial z} = 0, \frac{\partial Ey}{\partial z} = 0, \frac{\partial Ex}{\partial z} = 0$$

From equation, we can write two independent sets of coupled equations.

TM polarized field:

$$\frac{\partial Ex}{\partial t} = \frac{1}{\varepsilon}\frac{\partial Hz}{\partial y}$$

$$\frac{\partial Ey}{\partial t} = -\frac{1}{\varepsilon}\frac{\partial Hz}{\partial x}$$

$$\frac{\partial Hz}{\partial t} = \frac{1}{\mu}\left(\frac{\partial Ex}{\partial y} - \frac{\partial Ey}{\partial x}\right)$$

And TE polarized field:

$$\frac{\partial Hx}{\partial t} = -\frac{1}{\mu}\frac{\partial Ez}{\partial y}$$

$$\frac{\partial Hy}{\partial t} = \frac{1}{\mu}\frac{\partial Ez}{\partial x}$$

$$\frac{\partial Ez}{\partial t} = \frac{1}{\varepsilon}\left(\frac{\partial Hy}{\partial x} - \frac{\partial Hx}{\partial y}\right)$$

Utilizing Yee's spatial gridding scheme, the partial spatial derivatives in can be approximated by a central difference approximation in space. For example, equations respectively become

$$\frac{\partial E_x}{\partial t} = \frac{1}{\varepsilon}\frac{H_z(i,j) - H_z(i,j-1)}{\Delta y}$$

$$\frac{\partial E_y}{\partial t} = -\frac{1}{\varepsilon}\frac{H_z(i,j) - H_z(i-1,j)}{\Delta x}$$

$$\frac{\partial H_z}{\partial t} = \frac{1}{\mu}\left(\frac{E_x(i,j+1) - E_x(i,j)}{\Delta y} - \frac{E_y(i+1,j) - E_y(i,j)}{\Delta x}\right)$$

Yee's algorithm also utilizes central differencing in time for the *E* and *H* components. The *E* and *H* components are solved by using a leapfrog algorithm. All of the *E* components in the modeled space are computed and stored in memory by using the previously computed values of *E* and the newly computed *H* field data. At the next step, *H* is recomputed based on the previously obtained *H* and the newly updated *E*. This process continues until the time-stepping is terminated.

Applying central difference approximation equation) respectively, become

$$\frac{E_x^{n+1}\left(i+\frac{1}{2},j\right) - E_x^n\left(i+\frac{1}{2},j\right)}{\Delta t} = \frac{1}{\varepsilon}\frac{H_z^{n+\frac{1}{2}}\left(i+\frac{1}{2},j+\frac{1}{2}\right) - H_z^{n+\frac{1}{2}}\left(i+\frac{1}{2},j-\frac{1}{2}\right)}{\Delta y}$$

$$\frac{E_y^{n+1}\left(i,j+\frac{1}{2}\right)-E_y^n(i,j+\frac{1}{2})}{\Delta t}=-\frac{1}{\varepsilon}\frac{H_z^{n+\frac{1}{2}}\left(i+\frac{1}{2},j+\frac{1}{2}\right)-H_z^{n+\frac{1}{2}}\left(i-\frac{1}{2},j+\frac{1}{2}\right)}{\Delta y}$$

$$\frac{H_z^{n+\frac{1}{2}}\left(i+\frac{1}{2},j+\frac{1}{2}\right)-H_z^{n-\frac{1}{2}}(i+\frac{1}{2},j+\frac{1}{2})}{\Delta t}$$

$$=\frac{1}{\mu}\left(\frac{E_x^n\left(i+\frac{1}{2},j+1\right)-E_x^n\left(i+\frac{1}{2},j\right)}{\Delta y}-\frac{E_y^n\left(i+1,j+\frac{1}{2}\right)-E_y^n\left(i,j+\frac{1}{2}\right)}{\Delta x}\right)$$

To ensure the numerical stability of the Yee algorithm, it is required to set an upper bound of the time step, Δt, which is related with spatial increment Δx, Δy, and Δz in accordance with the Courant-Friedrich-Levy (CFL) stability condition. In three dimensions, the CFL condition is

$$\Delta t \le \Delta t_{max}=\frac{1}{c\sqrt{\frac{1}{\Delta x^2}+\frac{1}{\Delta y^2}+\frac{1}{\Delta z^2}}}$$

The upper bound on Δt in the above equation guarantees the stability of the algorithm, which is essential to guarantee its validity when applied to a wide variety of electromagnetic wave modeling problems.

CHAPTER 6

SIMULATION STRUCTURE

6.1 One-Dimensional Structure:

Detailed analysis of one dimensional structure has been shown here.

6.1.1 Vacuum (Permittivity 1) is used as a Material and PML doesn't use at the boundary:

A one – dimensional view of permittivity 1 structure was used for simulation is shown Fig.6.1. Cell 1 to 200 we use permittivity 1. PML doesn't used hare. A gaussian (700 T Hz) originate at 100^{th} cell. The simulation pulse is stroked on the boundary of the material. The pulse is reflected back from the boundary. Fig. 6.1 shows the propagation of the Gaussian pulse with 700 THz at different cell. After 225 iteration step the Gaussian pulse reflected back from the boundary.

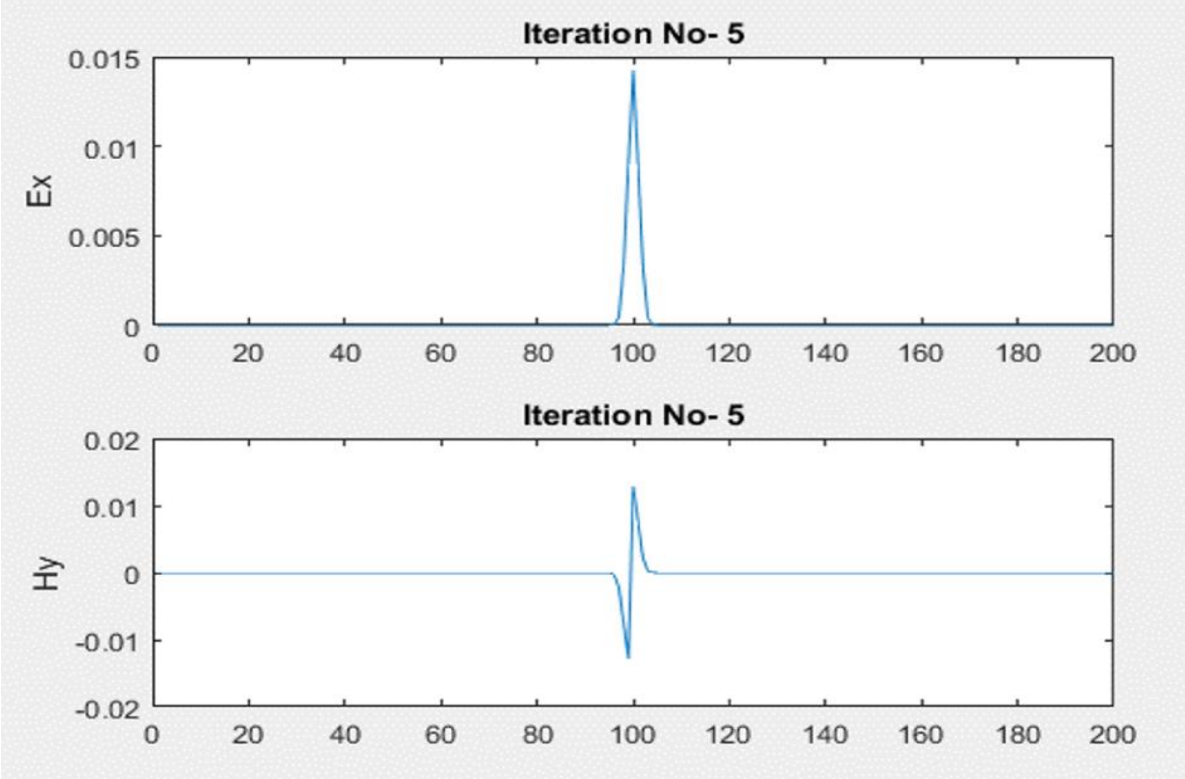

Fig.6.1: After 5 Iteration steps waveforms of Gaussian pulse.

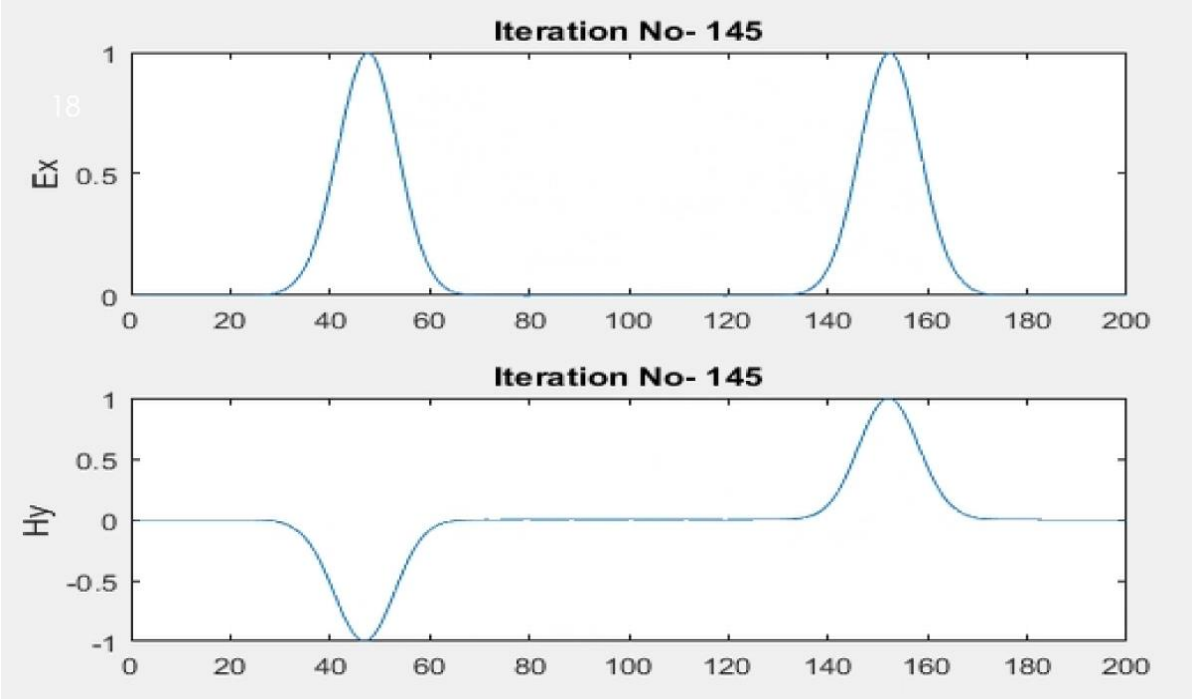

Fig.6.2: After 145 Iteration steps waveforms of Gaussian pulse

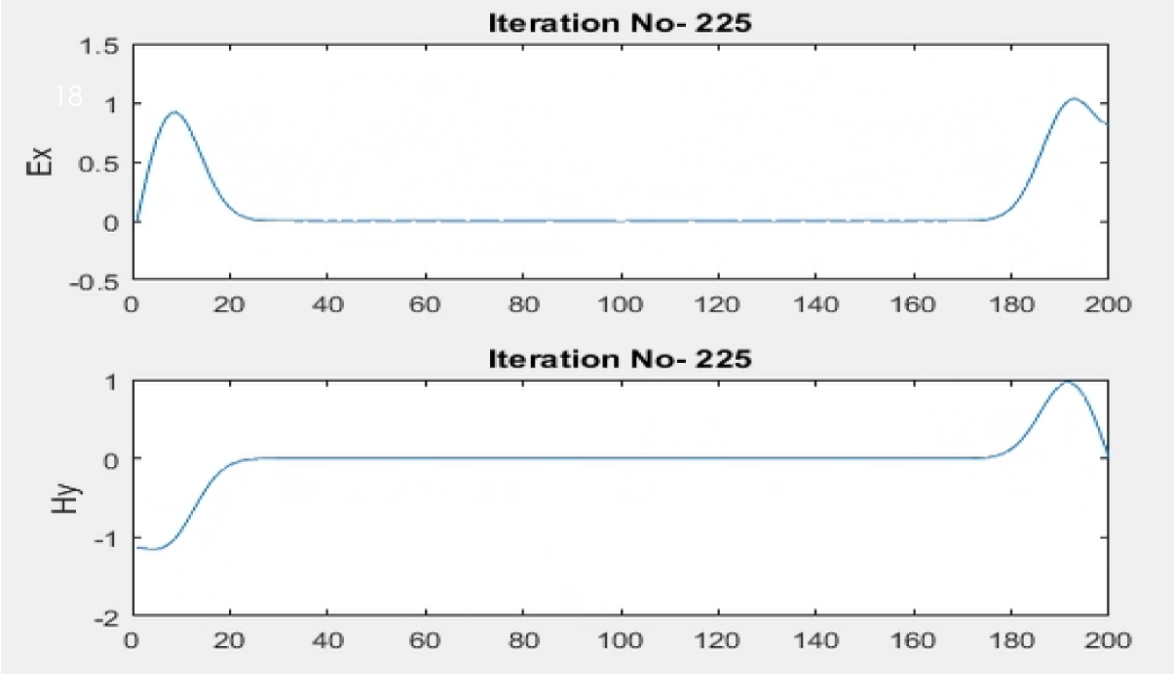

Fig.6.3: After 225 Iteration steps waveforms of Gaussian pulse

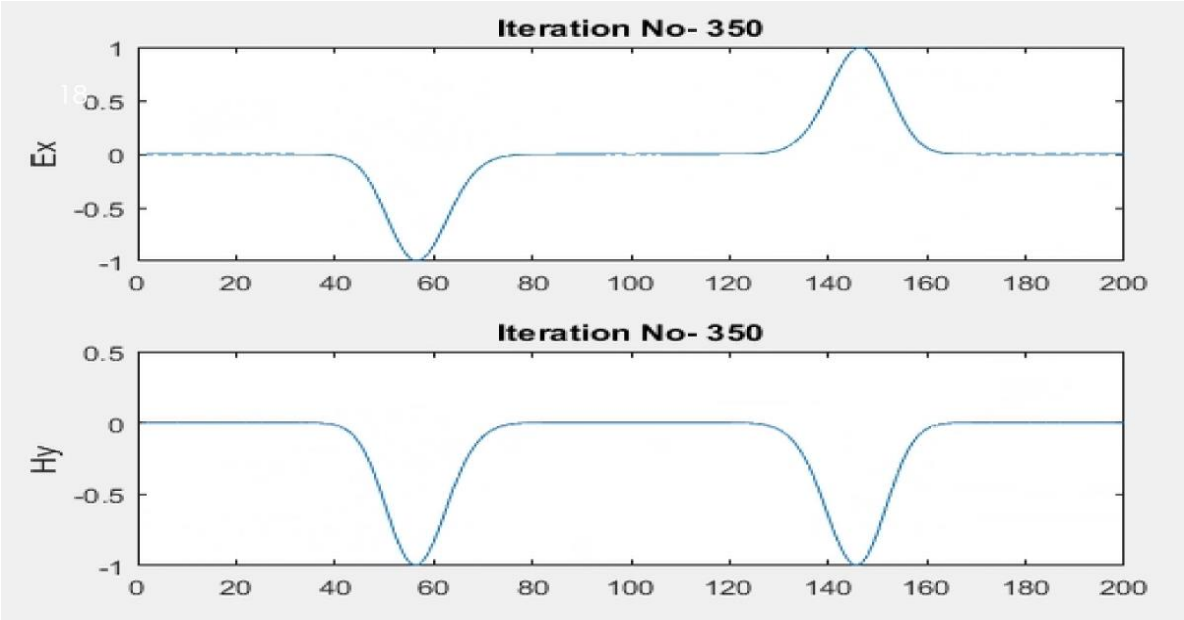

Fig.6.4: After 350 Iteration steps waveforms of Gaussian pulse

6.1.2 Air (Permittivity 1) is used as a Material and PML is used at the boundary:

A one – dimensional view of permittivity 1 structure was used for simulation is shown Fig.6.1. Cell 1 to 200 we use permittivity 1. PML is used hare. A gaussian pulse (700 T Hz) originate at 100^{th} cell. The simulation pulse is stroked on the boundary of the material. The pulse is absorbed by the boundary. Fig. 6.2 shows the propagation of the Gaussian pulse with 700 THz at different cell. After 260 iteration steps the Gaussian pulse absorbed by the boundary.

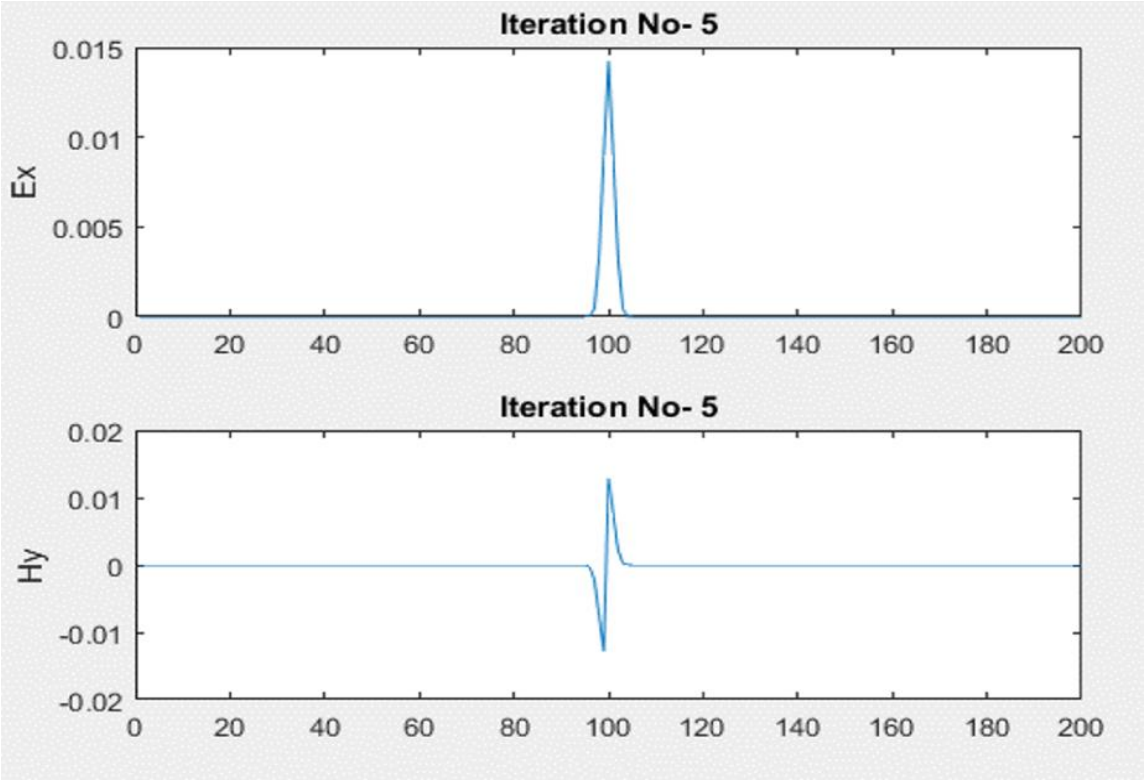

Fig.6.5: After 5 Iteration steps waveforms of Gaussian pulse

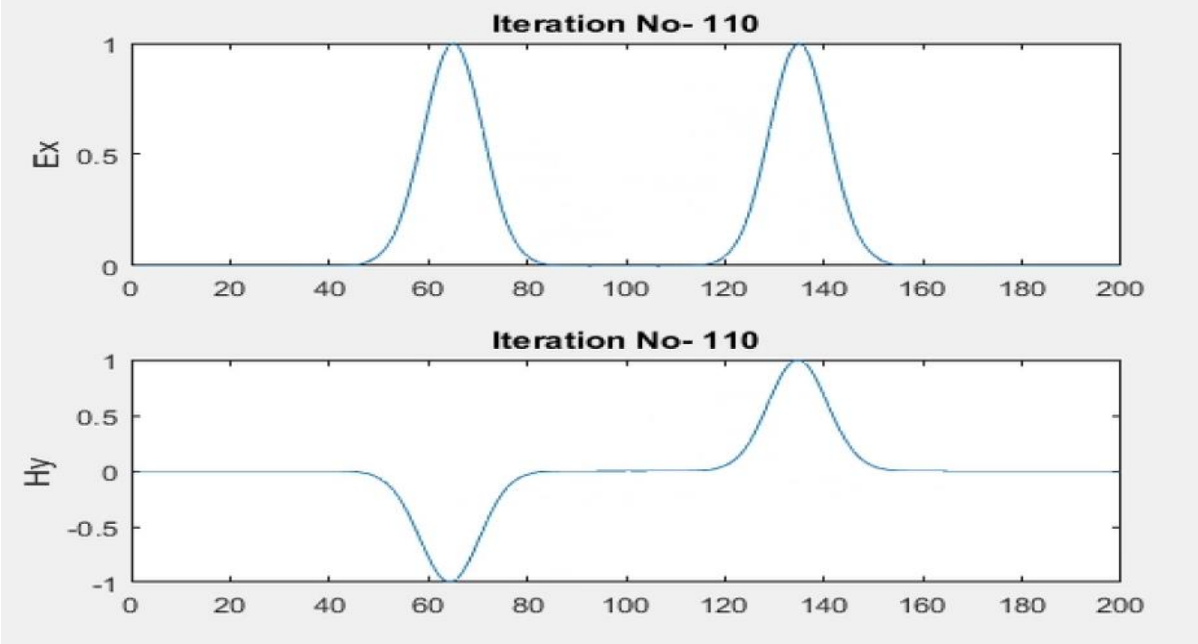

Fig.6.6: After 110 Iteration steps waveforms of Gaussian pulse

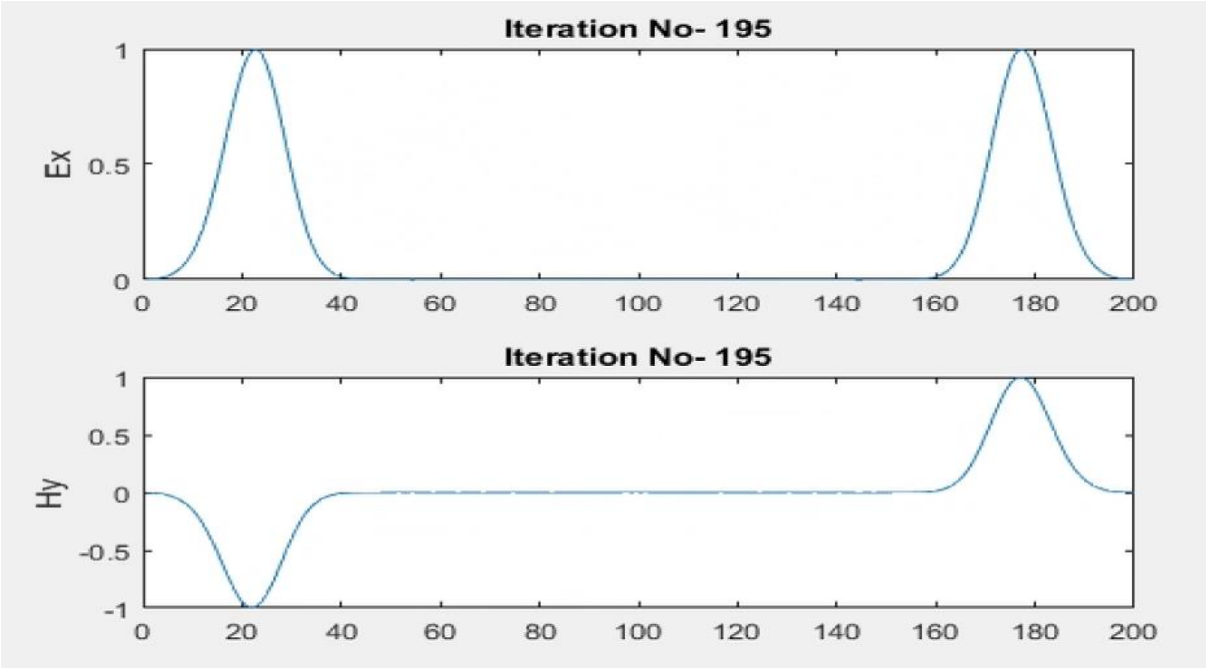

Fig.6.7: After 195 Iteration steps waveforms of Gaussian pulse

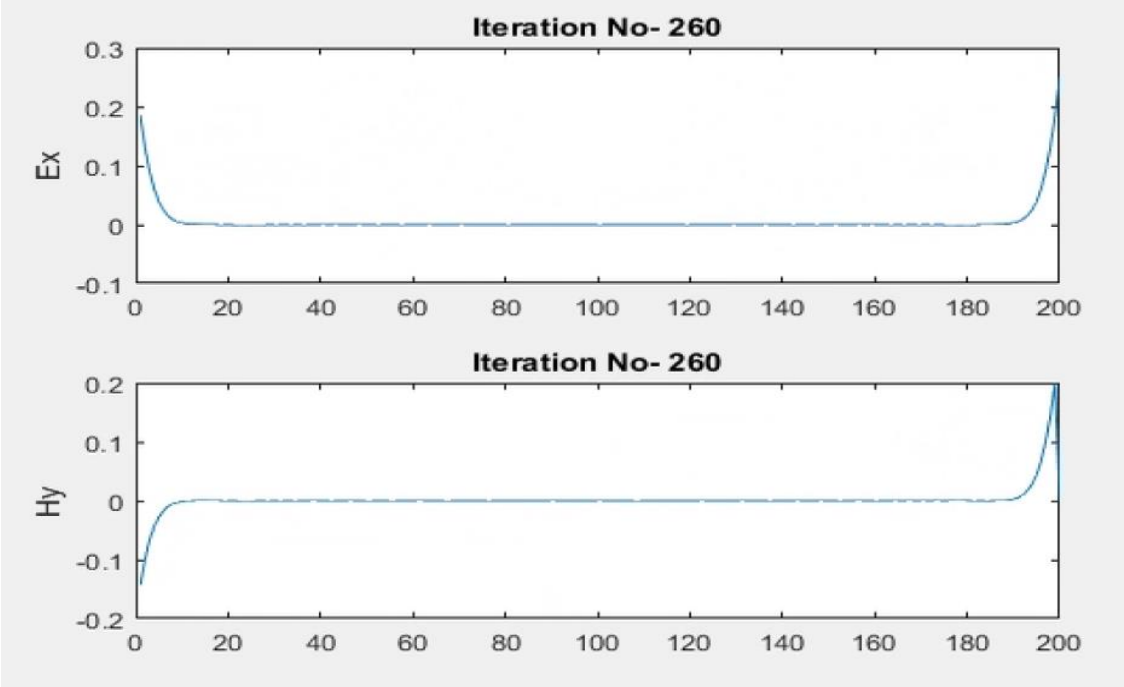

Fig.6.8: After 260 Iteration steps waveforms of Gaussian pulse

6.1.3 Different Permittivity (1 & 4) Material:

A one – dimensional view of single interface of permittivity 1 & 4 structure was used for simulation is shown Fig.6.1. permittivity 1 and permittivity 4 interface is made by putting a permittivity 1 layer on the top of permittivity 1 layer. Cell 1 to 100 we use permittivity 1 and cell 101 to 200 we use permittivity 4 material. PML is used hare. A gaussian (700 T Hz) originate at 0^{th} cell. The simulation pulse is stroked on the surface of two material. Some portion of the pulse is reflected back from the interface.

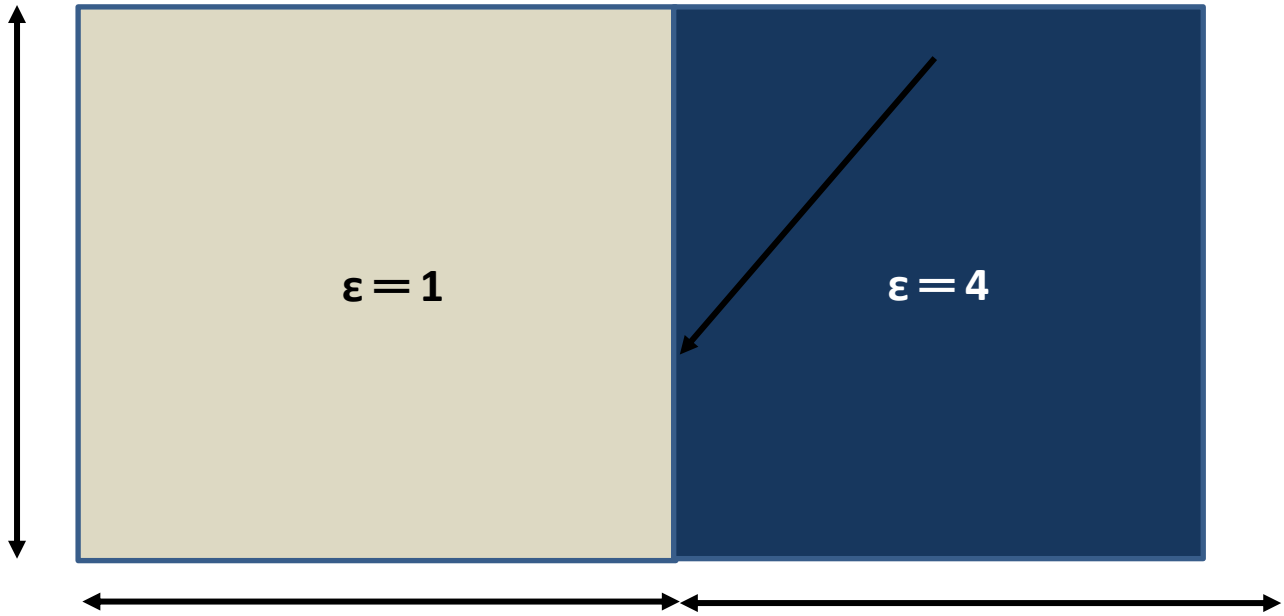

Fig.6.9: 0 to 100 cells have a relative permittivity of 1 while 101 to 200 cells have a relative permittivity of 4.

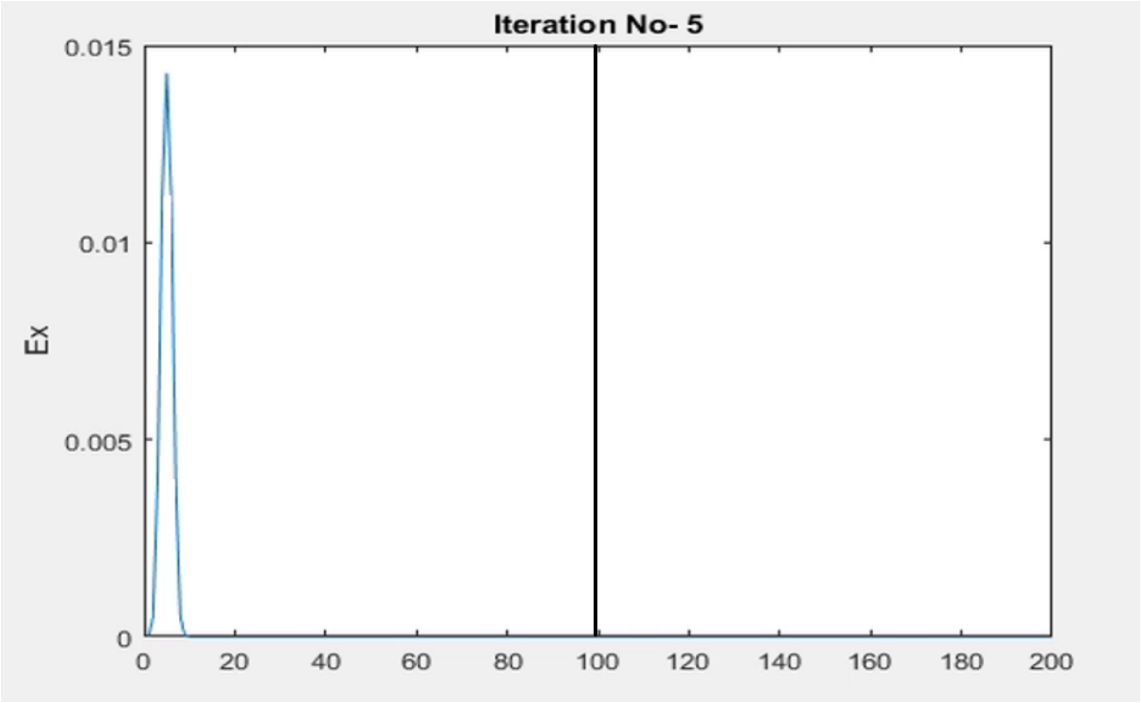

Fig.6.10: After 5 Iteration steps waveforms of Gaussian pulse

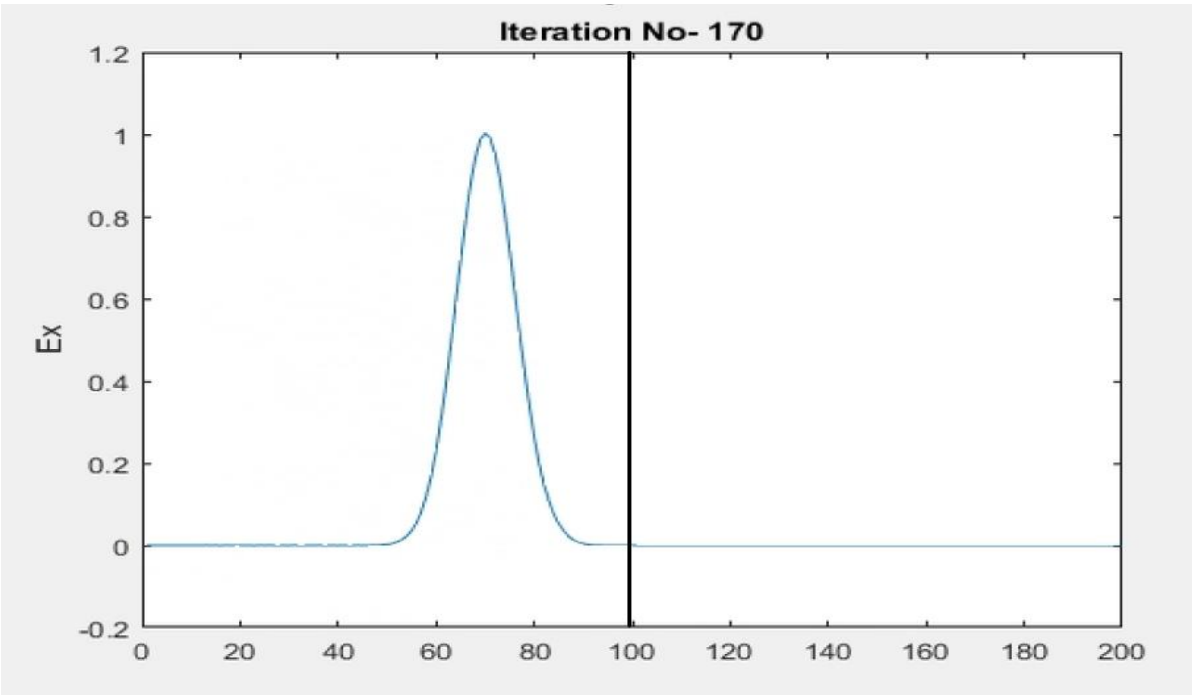

Fig.6.11: After 170 Iteration steps waveforms of Gaussian pulse

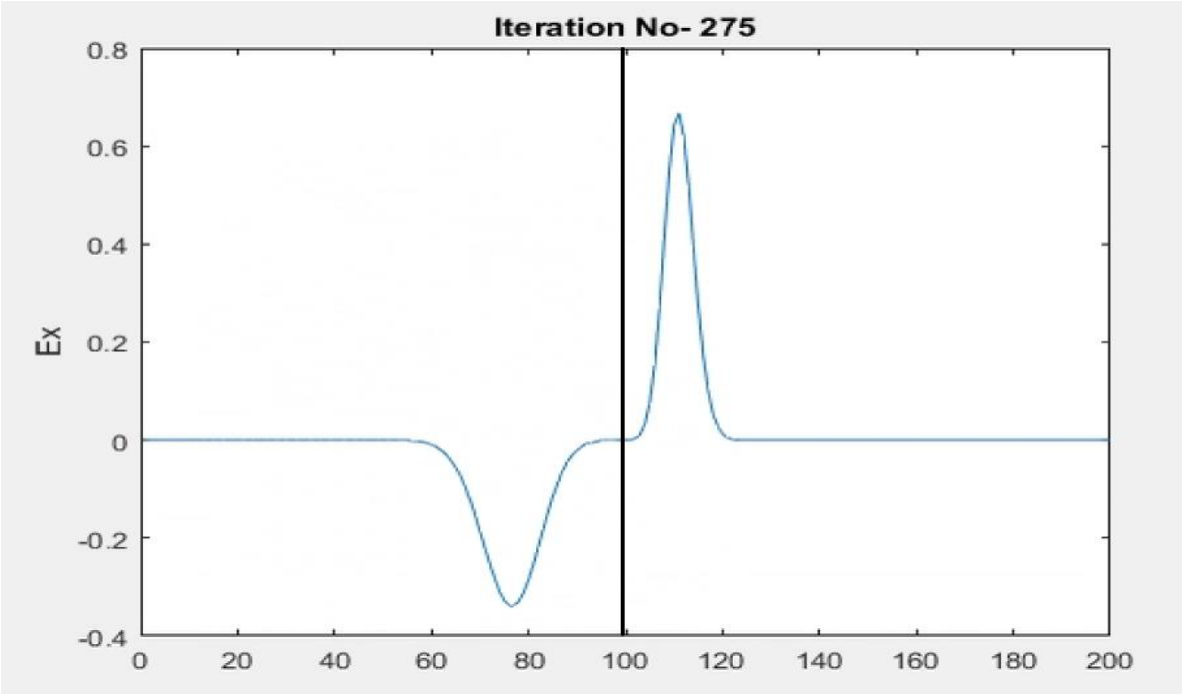

Fig.6.12: After 275 Iteration steps waveforms of Gaussian pulse

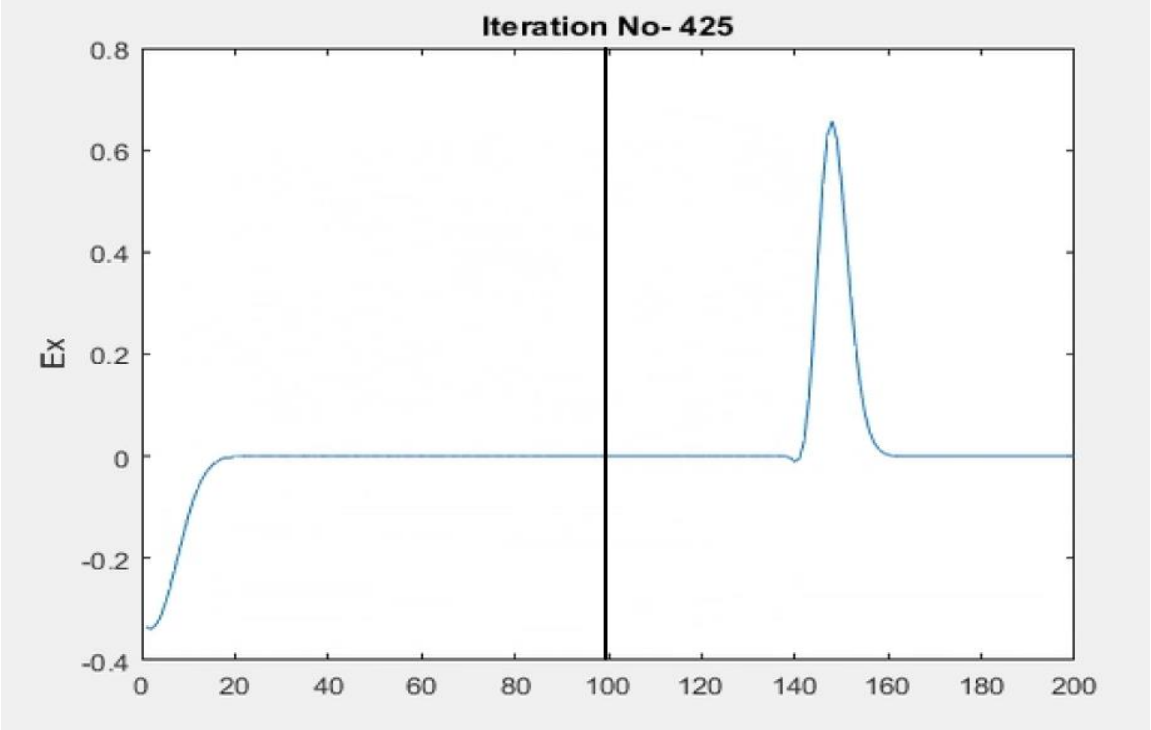

Fig.6.13: After 425 Iteration steps waveforms of Gaussian pulse

6.2 Two-Dimensional Structure:

6.2.1 Vacuum (Permittivity 1) is used as a Material and PML doesn't use at the boundary:

A two – dimensional view of permittivity 1 structure was used for simulation is shown Fig.6.4. Cell 1 to 500 along x-axis and cell 1 to 500 along y-axis we use permittivity 1. PML doesn't used hare. A gaussian (700 T Hz) originate at (250,250) cell. The simulation pulse is stroked on the boundary of the material. The pulse is reflected back from the boundary. Fig. 6.4 shows the propagation of the Gaussian pulse with 700 THz at different cell. After 650 iteration steps the Gaussian pulse reflected back from the boundary.

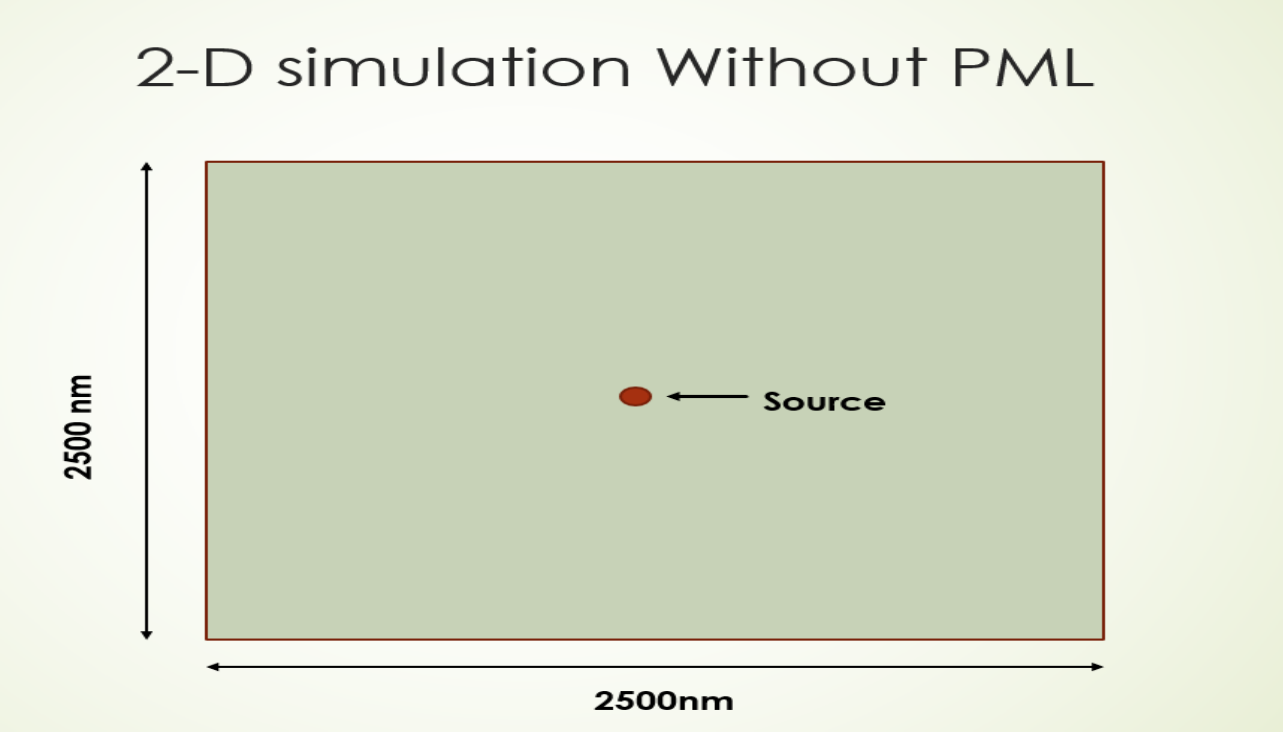

Fig.6.14: Cell 1 to 500 along x-axis and cell 1 to 500 along y-axis we use permittivity 1.

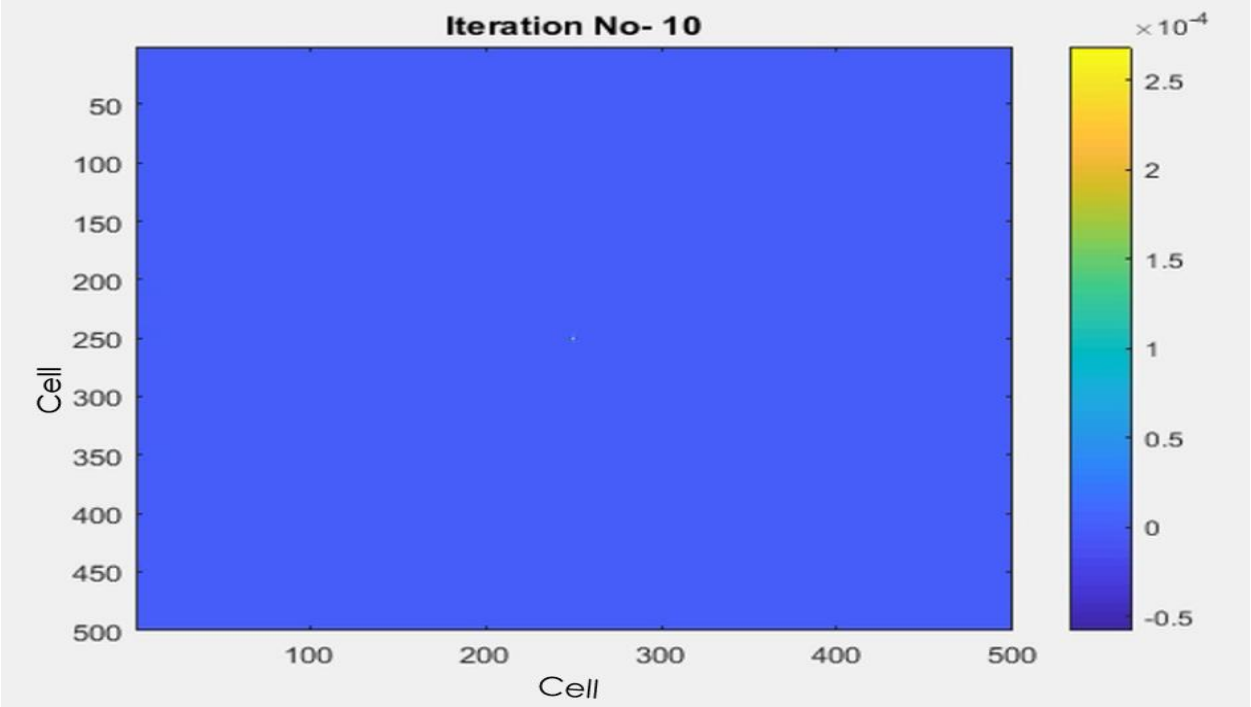

Fig.6.15: After 10 Iteration steps waveforms of the pulse.

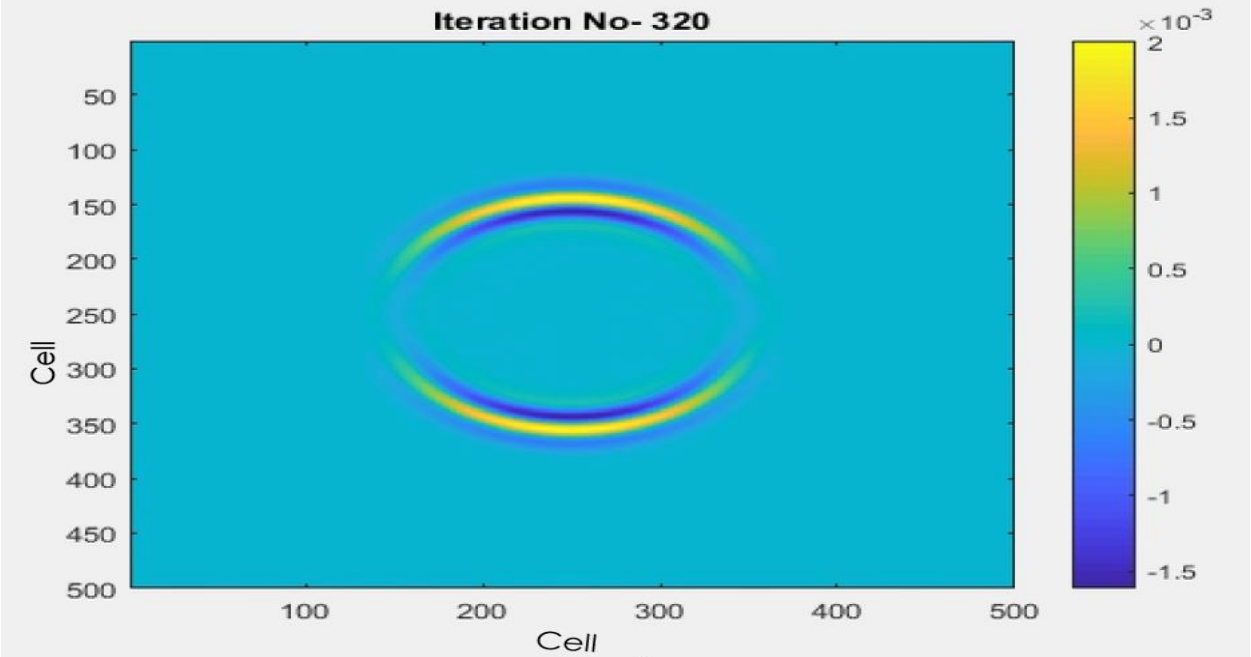

Fig.6.16: After 320 Iteration steps waveforms of the pulse.

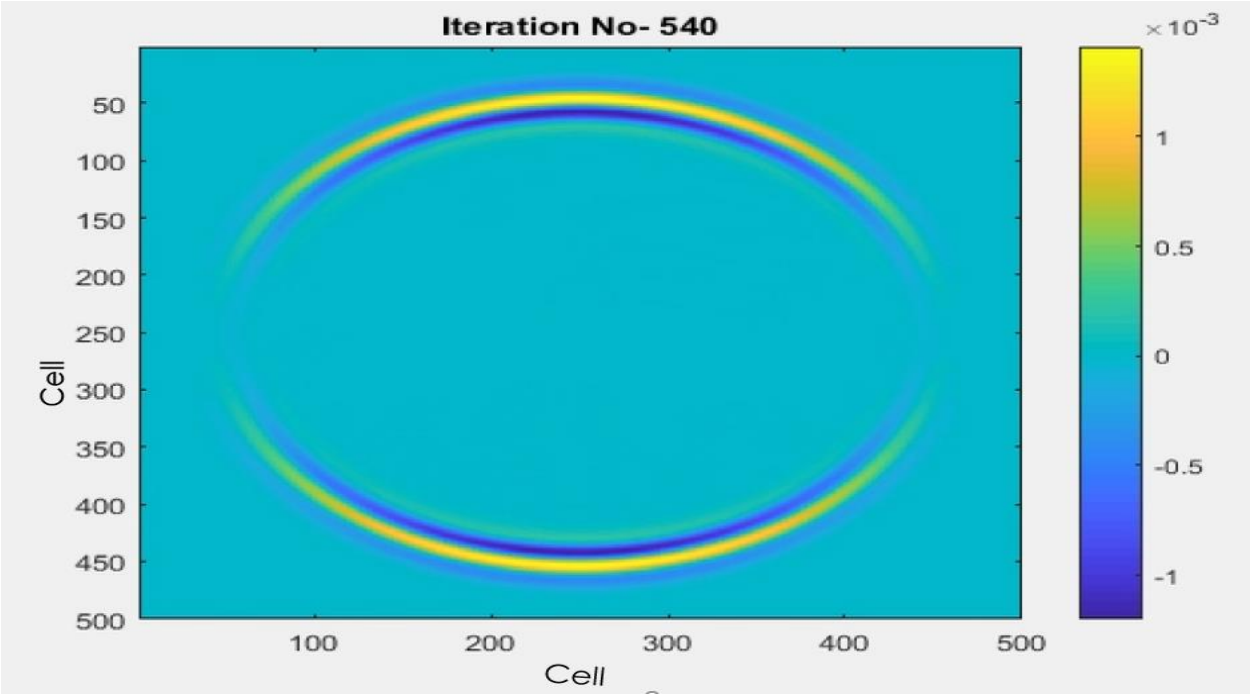

Fig.6.17: After 540 Iteration steps waveforms of the pulse.

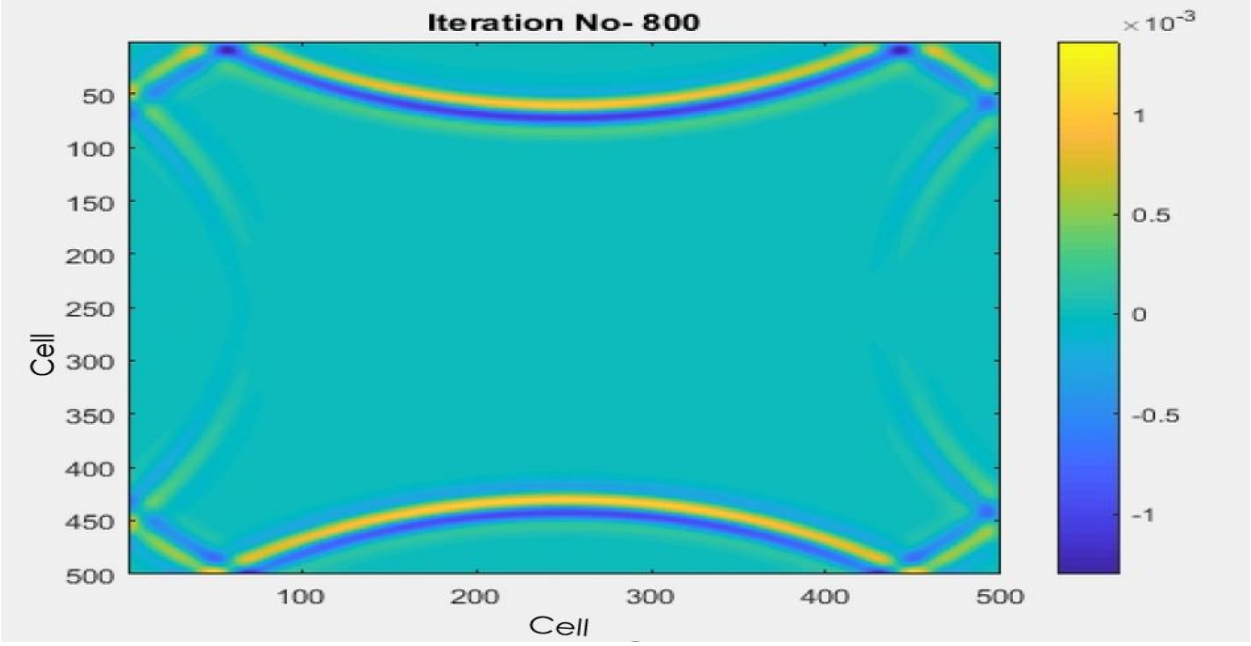

Fig.6.18: After 800 Iteration steps waveforms of the pulse.

6.2.2 Vacuum (Permittivity 1) is used as a Material and PML is used at the boundary:

A two – dimensional view of permittivity 1 structure was used for simulation is shown Fig.6.5. Cell 9 to 486 along x-axis and cell 9 to 486 along y-axis we use permittivity 1. And 8 cells at the boundary we used PML. A gaussian (700 T Hz) originate at (250,250) cell. The simulation pulse is stroked on the boundary of the material. The pulse is absorbed by the boundary. Fig. 6.5 shows the propagation of the Gaussian pulse with 700 THz at different cell. After 1350 iteration steps the Gaussian pulse is absorbed by the boundary.

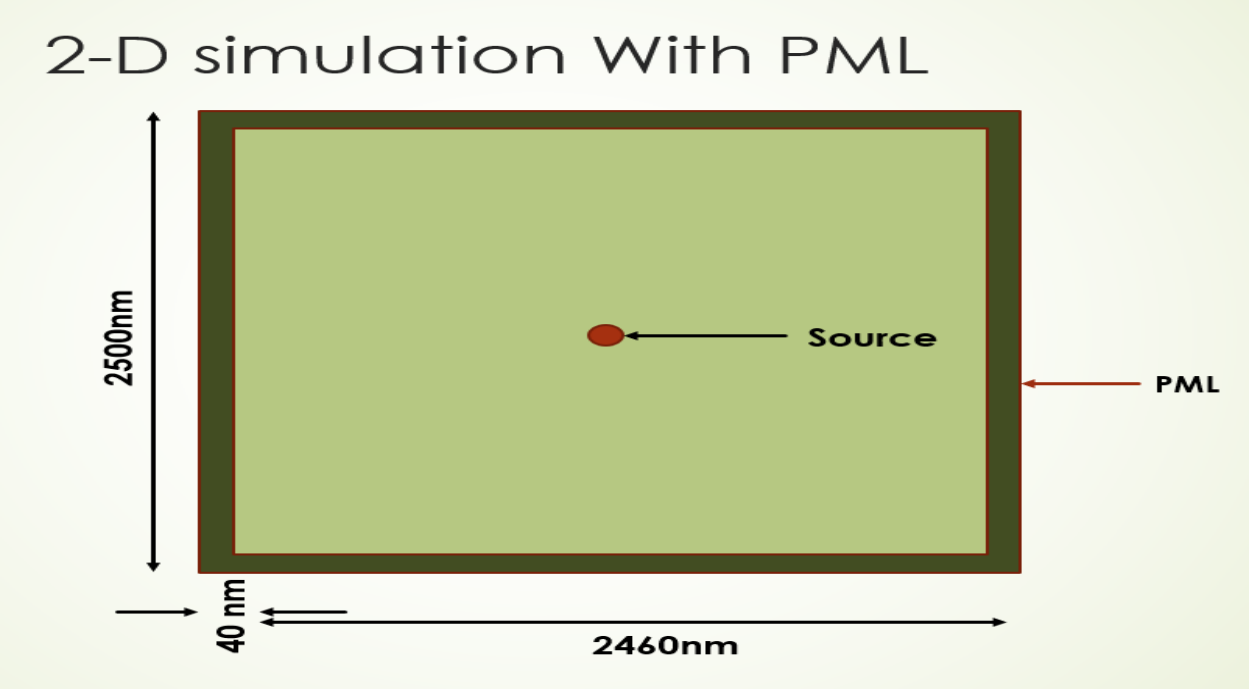

Fig.6.19: Cell 9 to 492 along x-axis and cell 9 to 486 along y-axis we use permittivity 1. And 8 cells at the boundary we used PML.

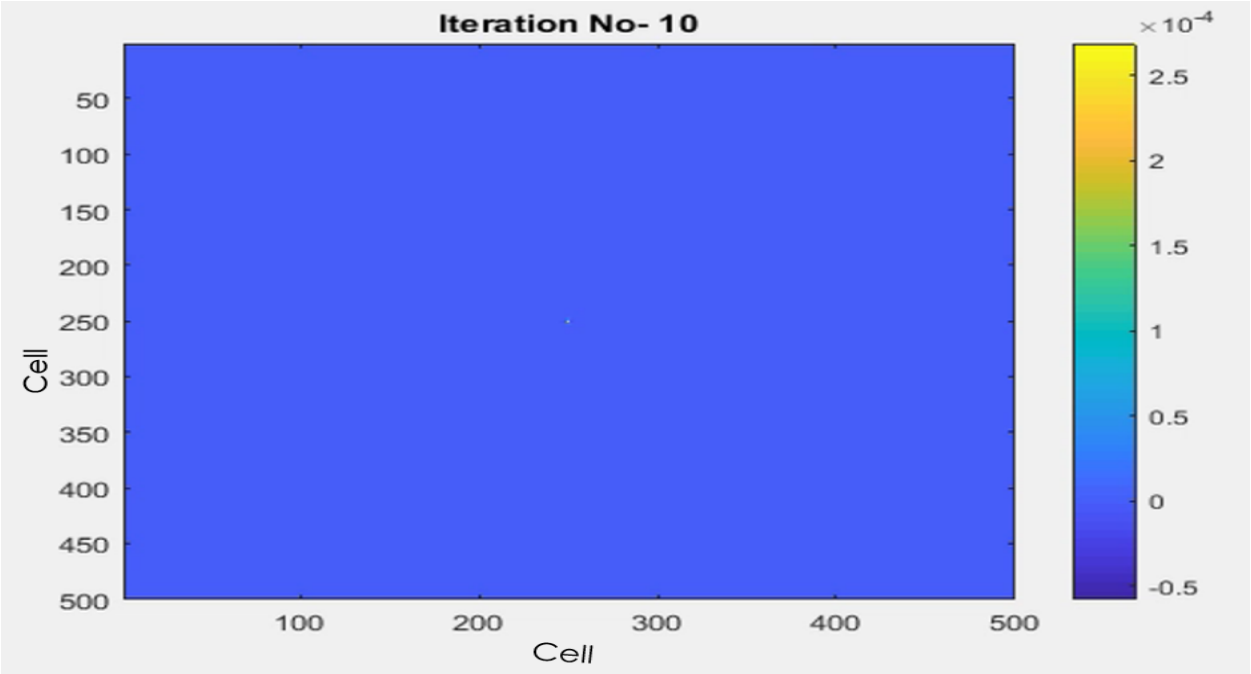

Fig.6.20: After 10 Iteration steps waveforms of the pulse.

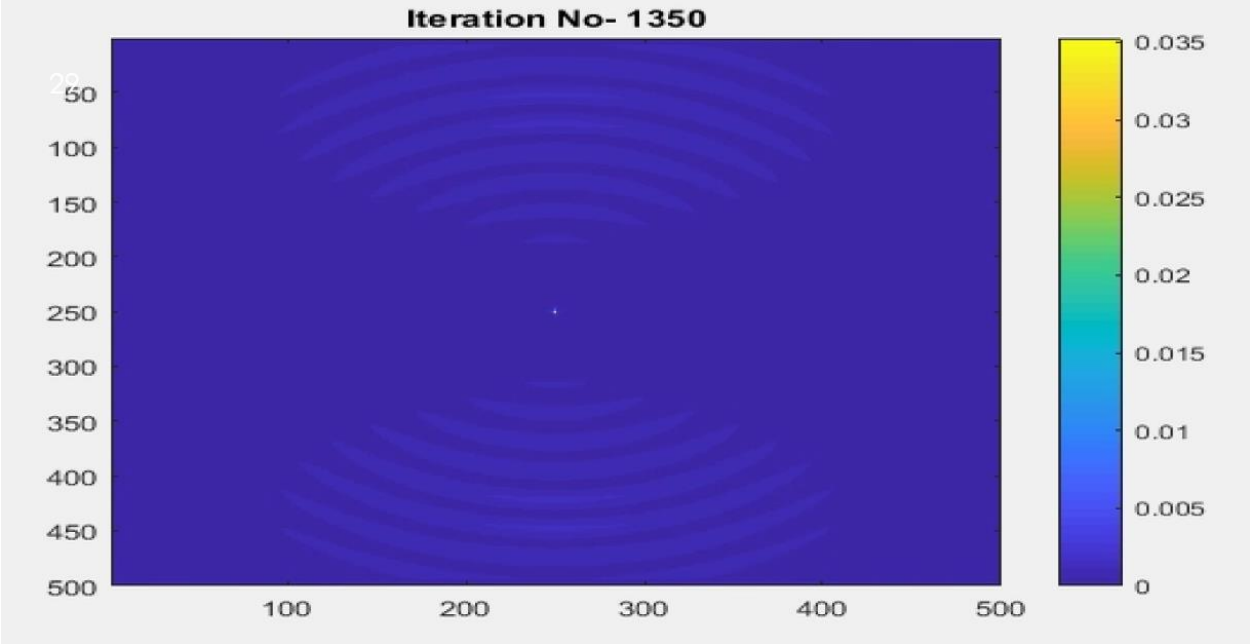

Fig.6.21: After 1350 Iteration steps waveforms of the pulse.

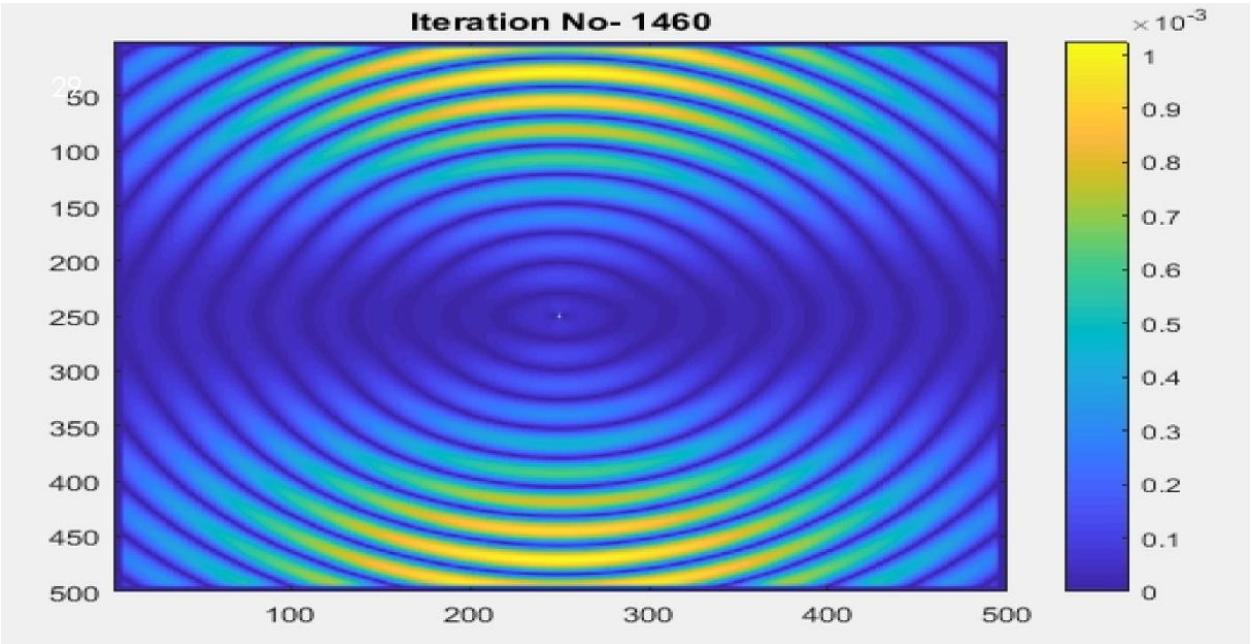

Fig.6.22: After 1460 Iteration steps waveforms of the pulse.

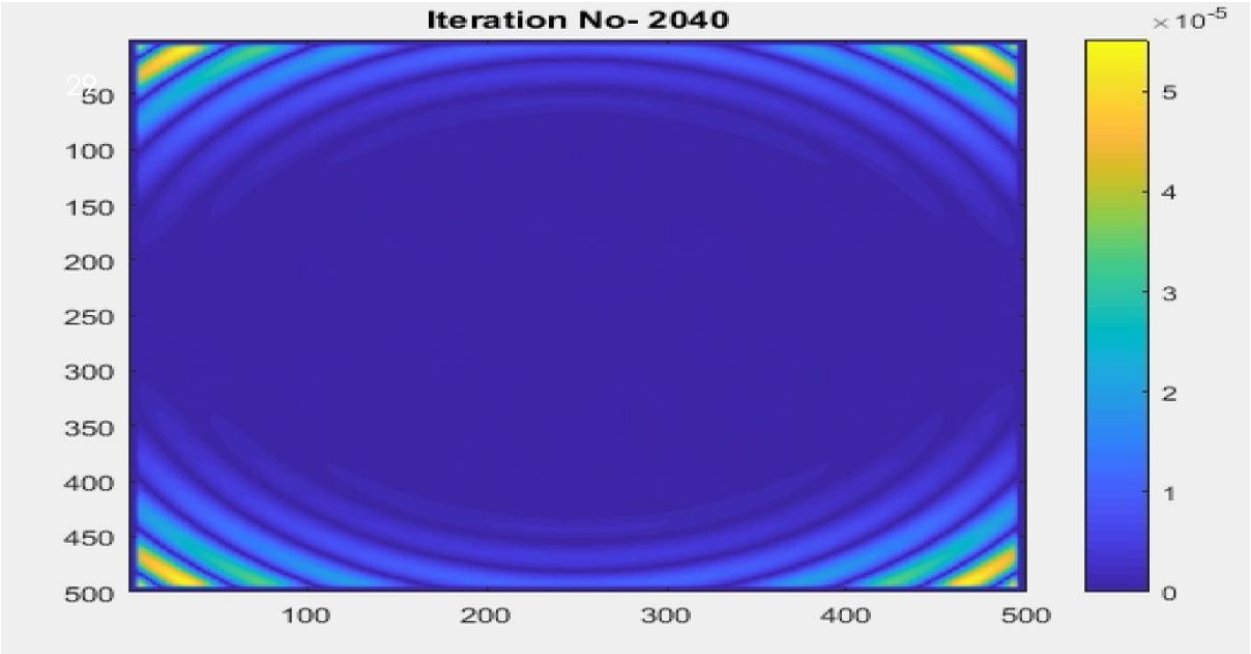

Fig.6.23: After 2040 Iteration steps waveforms of the pulse.

6.2.3 Single interface of Silver and Vacuum (Permittivity 1):

A two – dimensional view of single interface of silver & vacuum was used for simulation is shown Fig.6.6. silver and vacuum interface is made by putting a vacuum layer on the top of silver layer. Cell 1 to 500 we use silver and cell 501 to 1000 along x-axis we use vacuum as a material. PML is used hare. A gaussian (700 T Hz) is generated in vacuum close to the interface of both materials. SSP was generated here. Fig. 6.6 shows the propagation of the SSP at the interface of both materials.

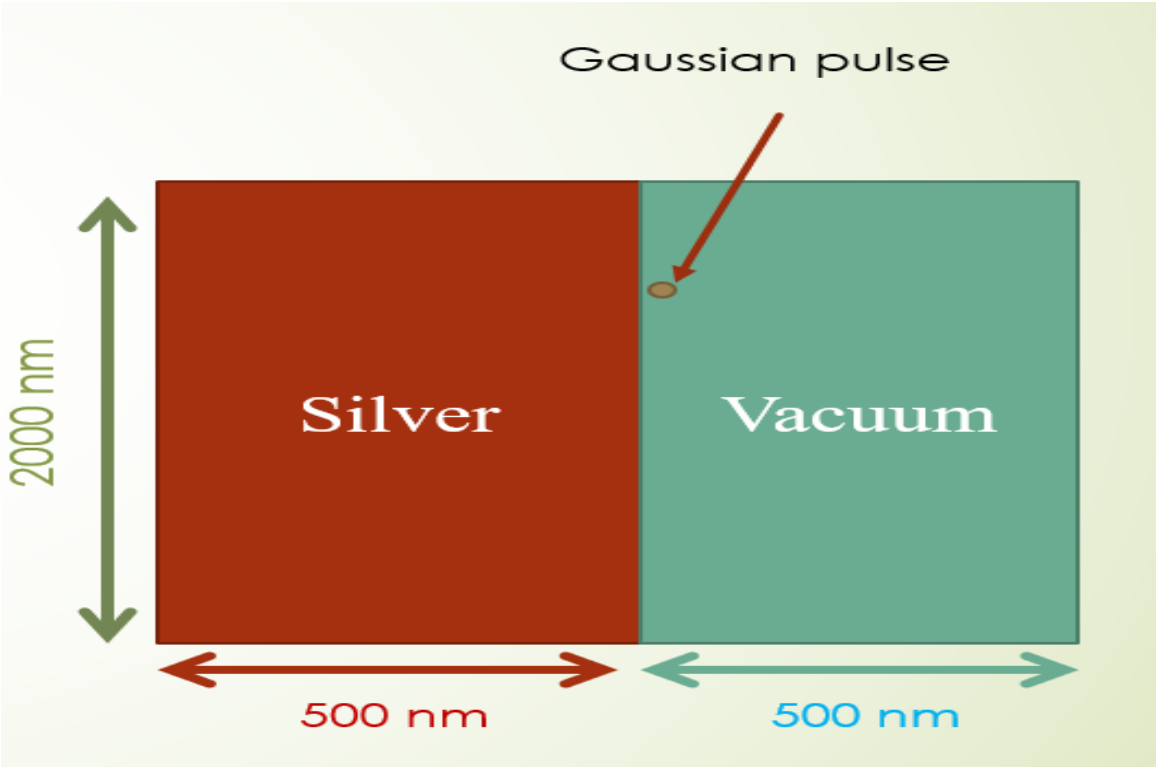

Fig.6.24: 0 to 500 cells have silver while 501 to 1000 cells along x-axis have vacuum as a material.

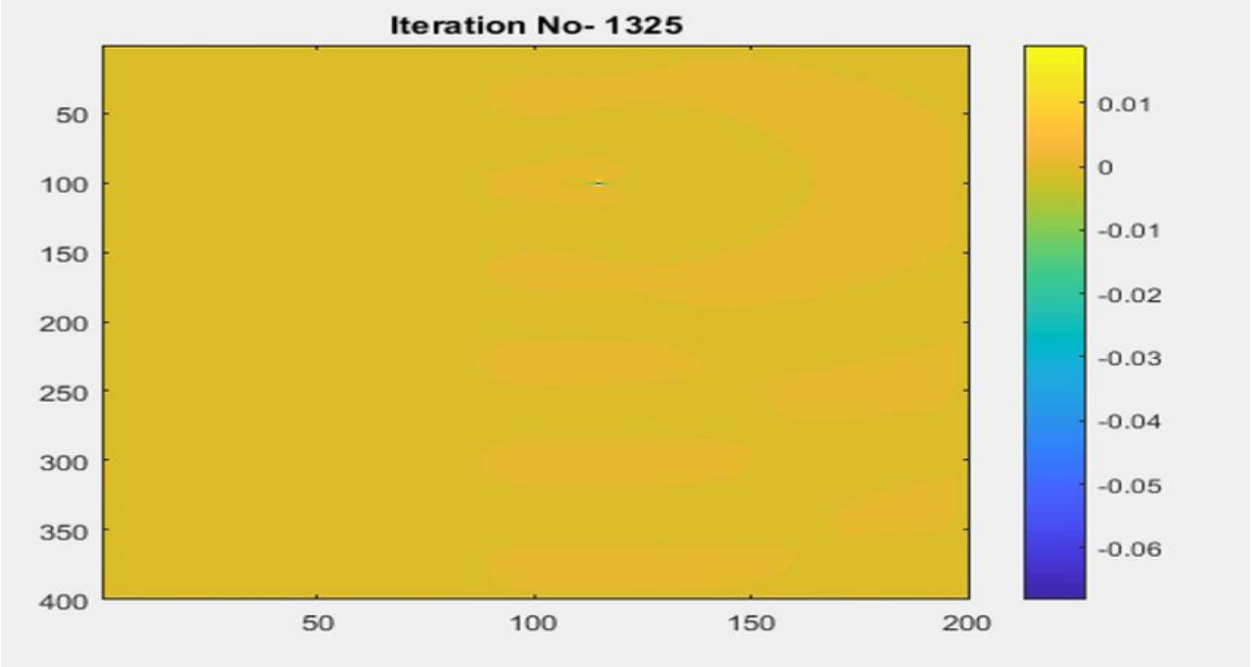

Fig.6.25: After 1325 Iteration steps waveforms of the SSP.

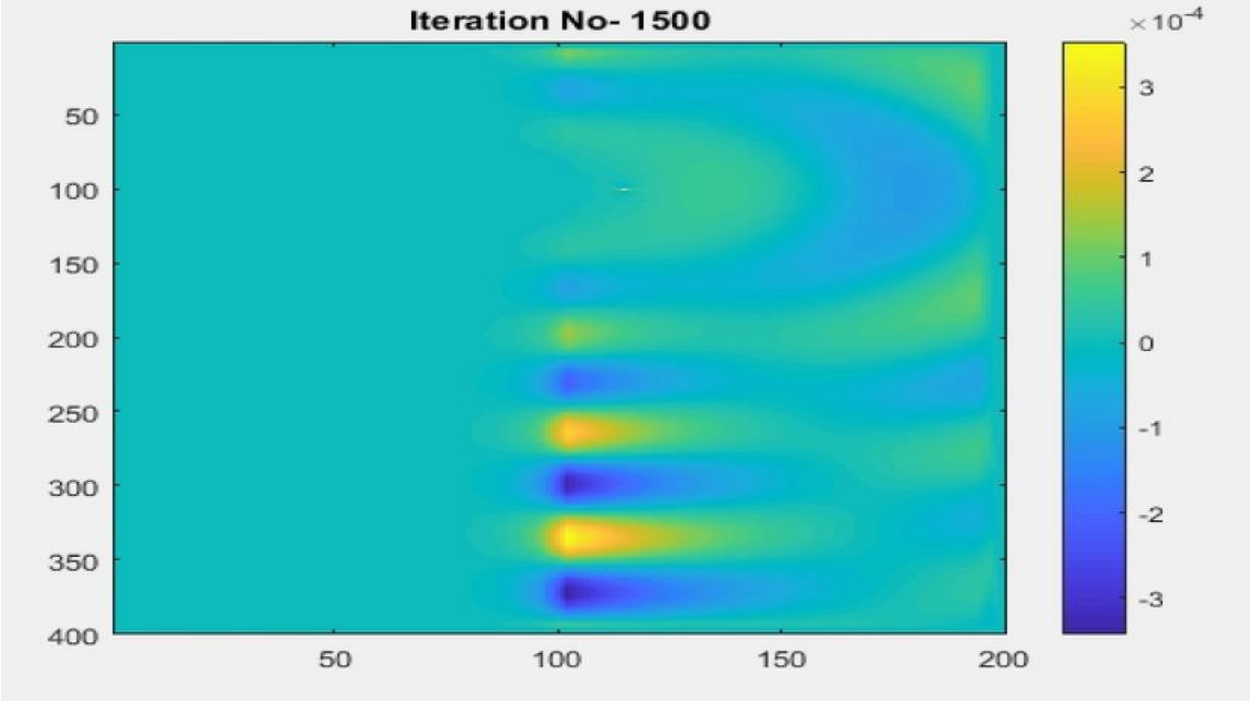

Fig.6.26: After 1500 Iteration steps waveforms of the SSP.

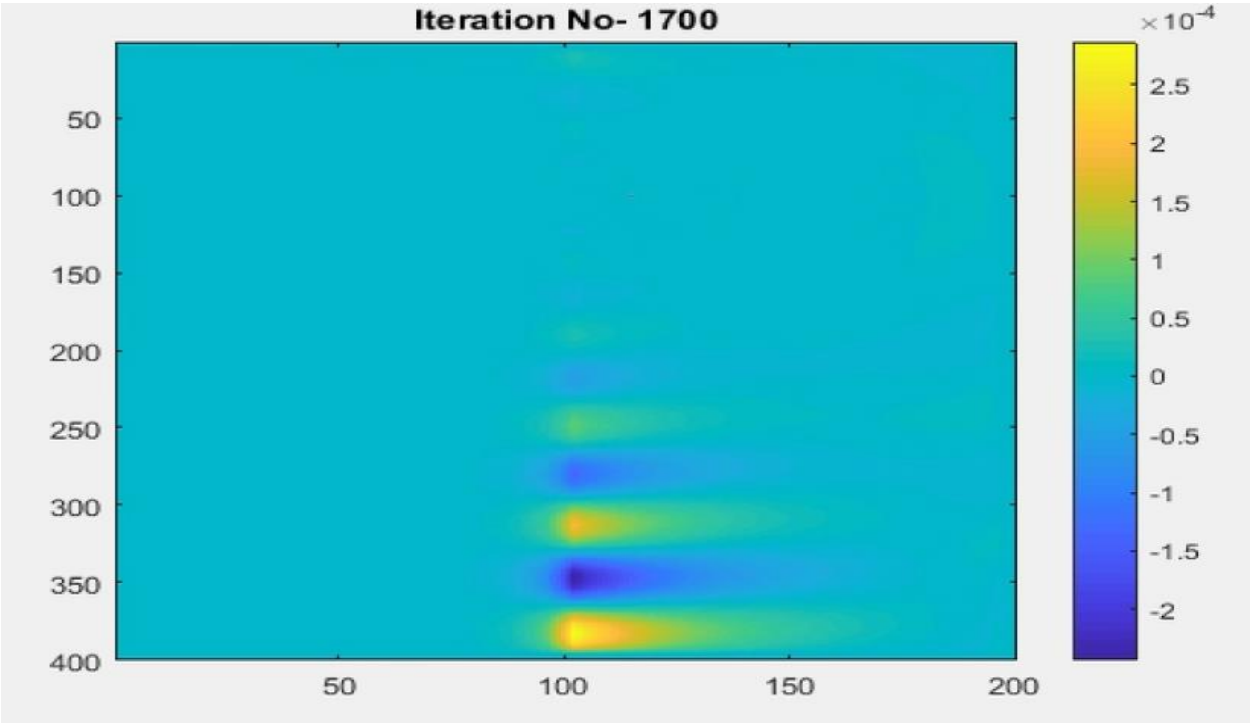

Fig.6.27: After 1700 Iteration steps waveforms of the SSP.

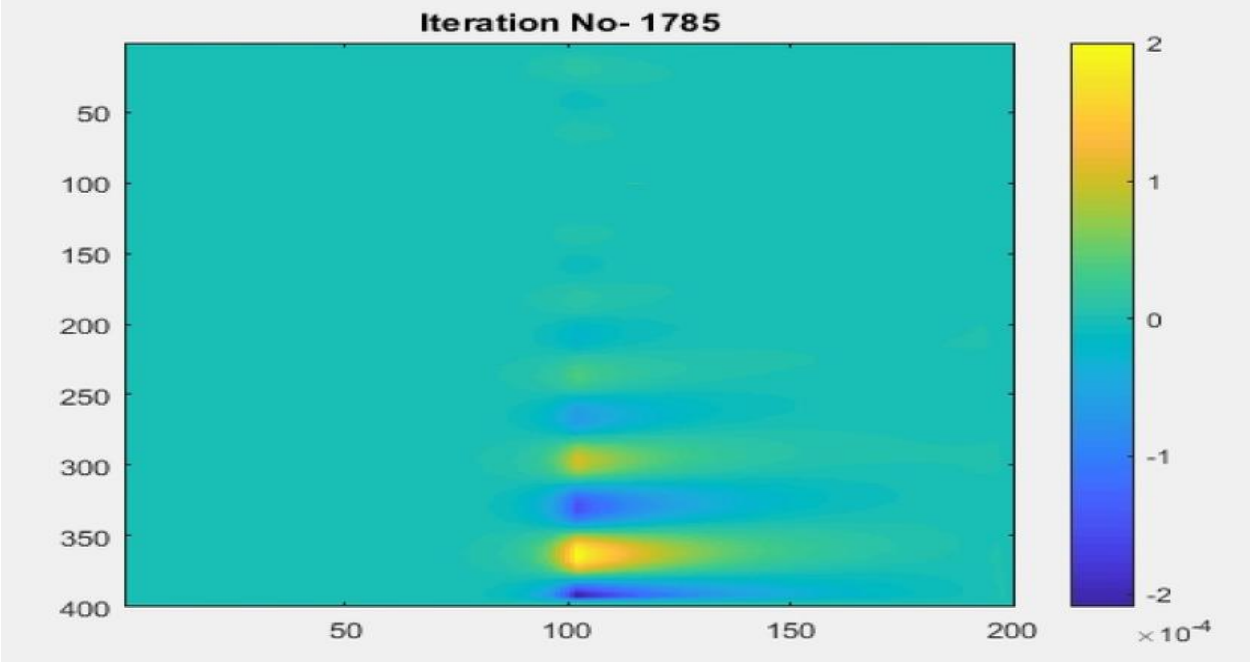

Fig.6.28: After 1785 Iteration steps waveforms of the SSP.

6.2.4 Single interface of Silver and Vacuum (Permittivity 1) and pumped the profile from the bottom end of the interface of both materials:

A two – dimensional view of single interface of silver & vacuum was used for simulation is shown Fig.6.6. silver and vacuum interface is made by putting a vacuum layer on the top of silver layer. Cell 1 to 500 we use silver and cell 501 to 1000 along x-axis we use vacuum as a material. PML is used hare. A gaussian (700 T Hz) is pumped the profile from the bottom end of the interface of both materials. SSP was generated here. Fig. 6.7 shows the propagation of the SSP at the interface of both materials.

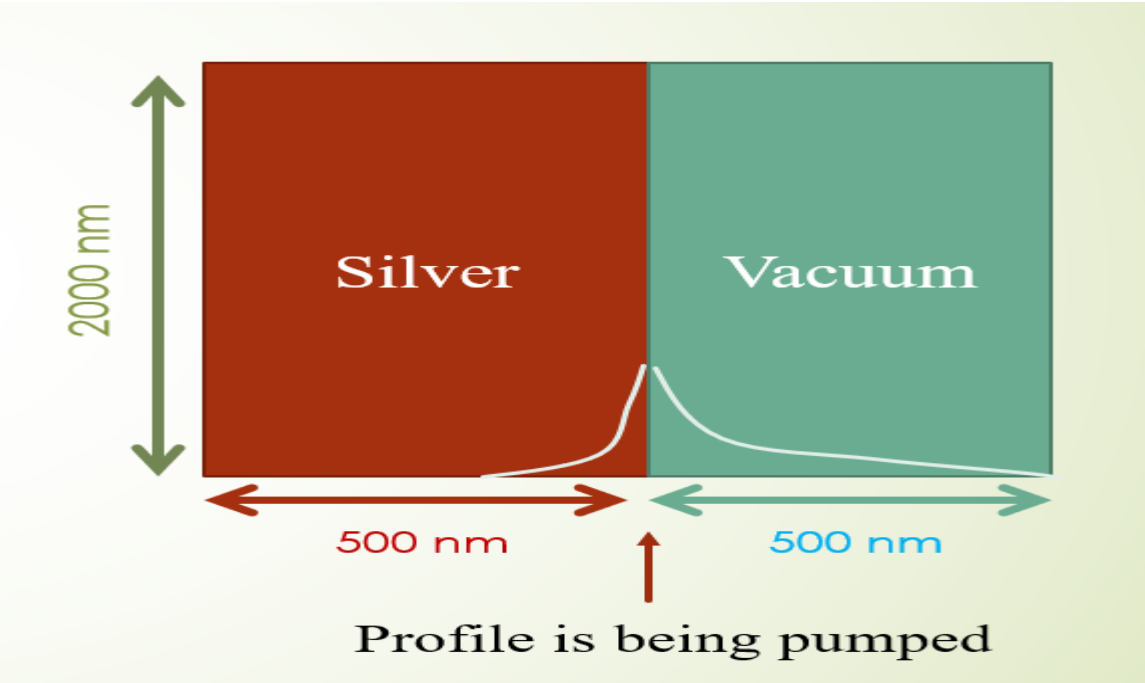

Fig.6.29: 0 to 500 cells have silver while 501 to 1000 cells along x-axis have vacuum as a material and a gaussian (700 T Hz) is pumped the profile from the bottom end of the interface of both materials

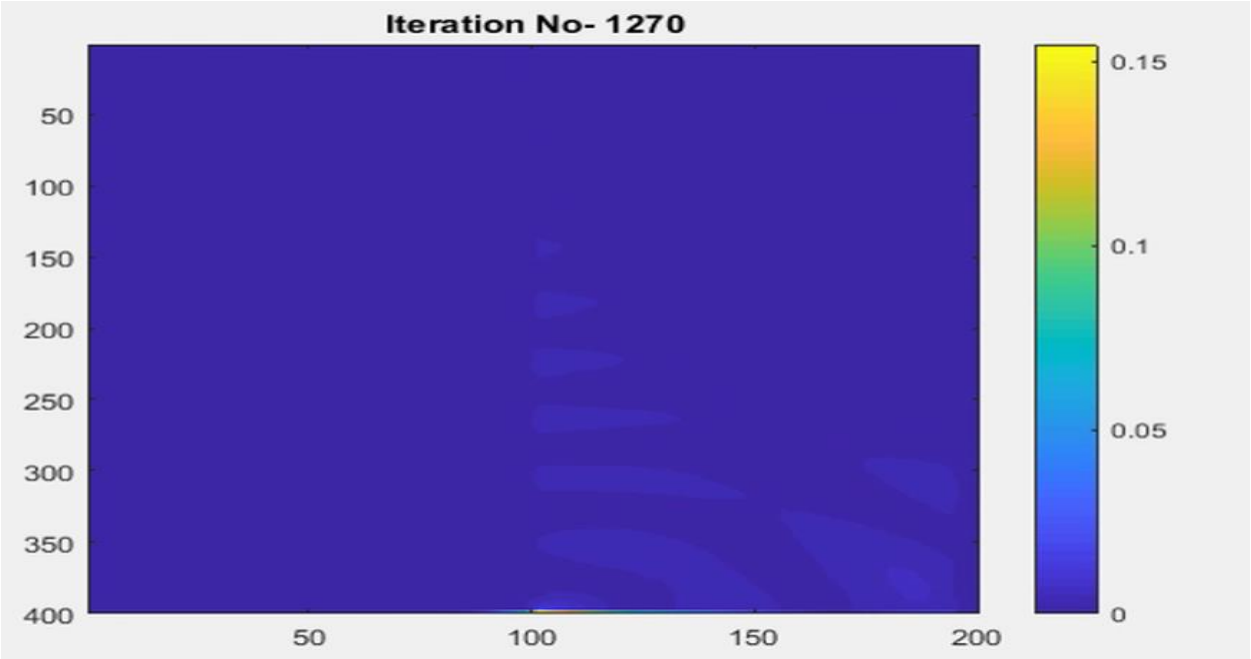

Fig.6.30: After 1270 Iteration steps waveforms of the SSP.

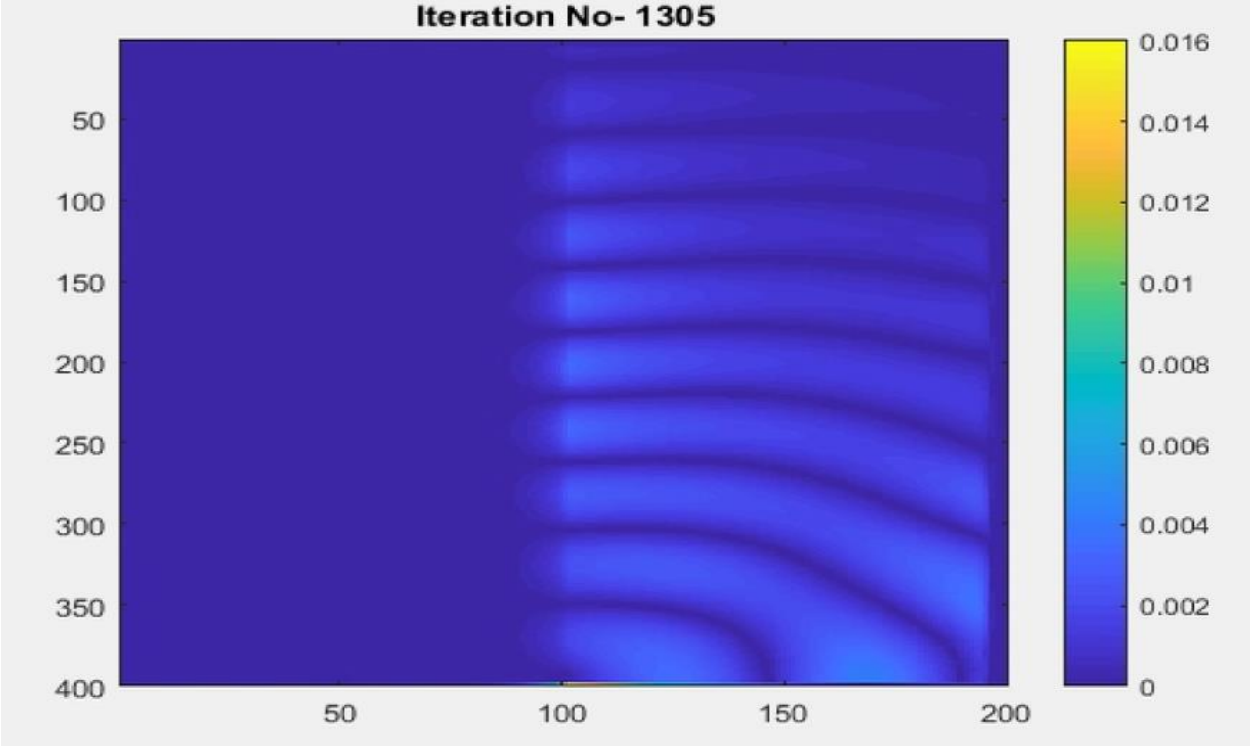

Fig.6.31: After 1305 Iteration steps waveforms of the SSP.

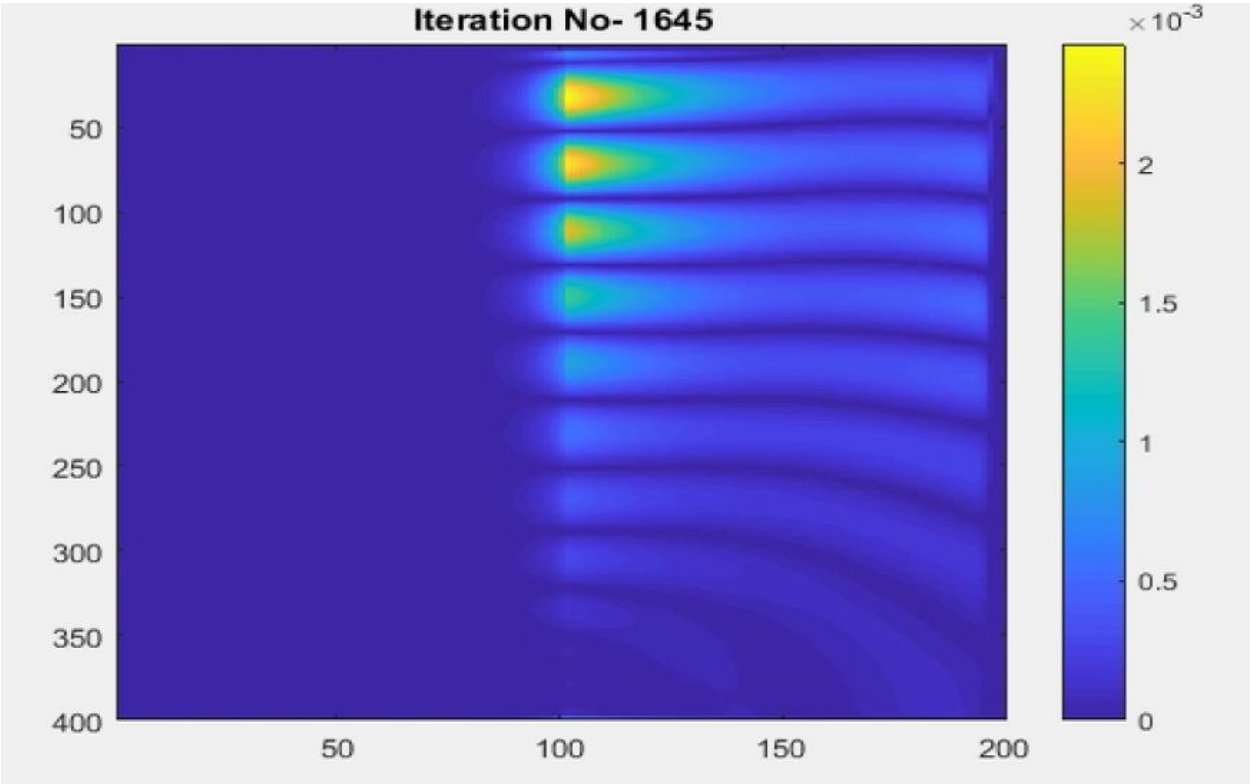

Fig.6.32: After 1645 Iteration steps waveforms of the SSP.

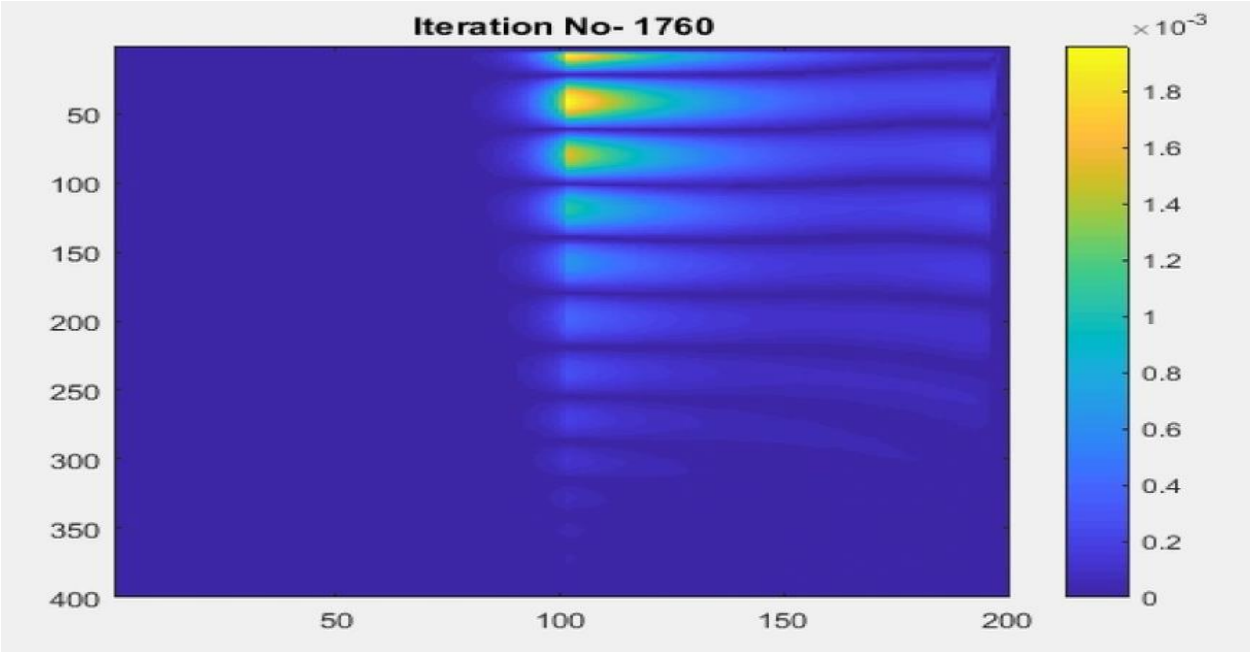

Fig.6.33: After 1760 Iteration steps waveforms of the SSP.

6.3 Three-Dimensional Structure:

6.3.1 3D Structure of Single interface of Silver and InP:

A three-dimensional view of the single interface Ag-InP structure that was used for the simulation is presented in Fig.6.7. Metal-dielectric interface is made by putting a thin silver film on the top of the bulk InP layer. Here a, b and c represent the length, width, and height of the InP layer while p, q and r represent the length, width, and height of the Ag layer respectively. The length of the InP and Ag layers have been kept fixed (a = p = 1000nm) while we vary both height (c) and width

(b) of InP layer. The dimensions of the structure are taken considering various applications in the plasmonic field [23, 24]

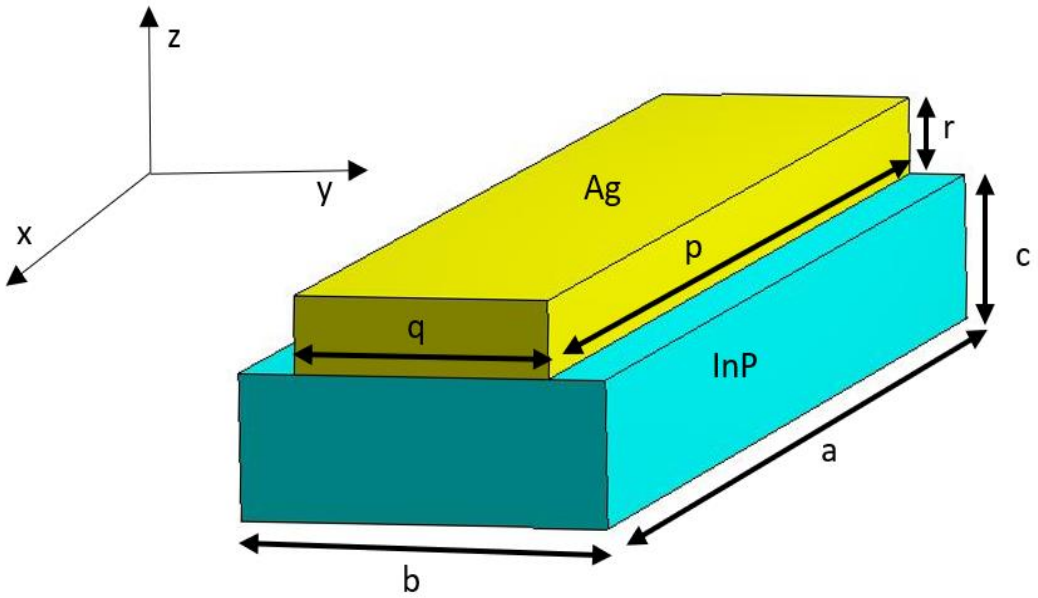

Fig. 6.34: Schematic diagram of the nanoplasmonic structure used for the numerical analysis.

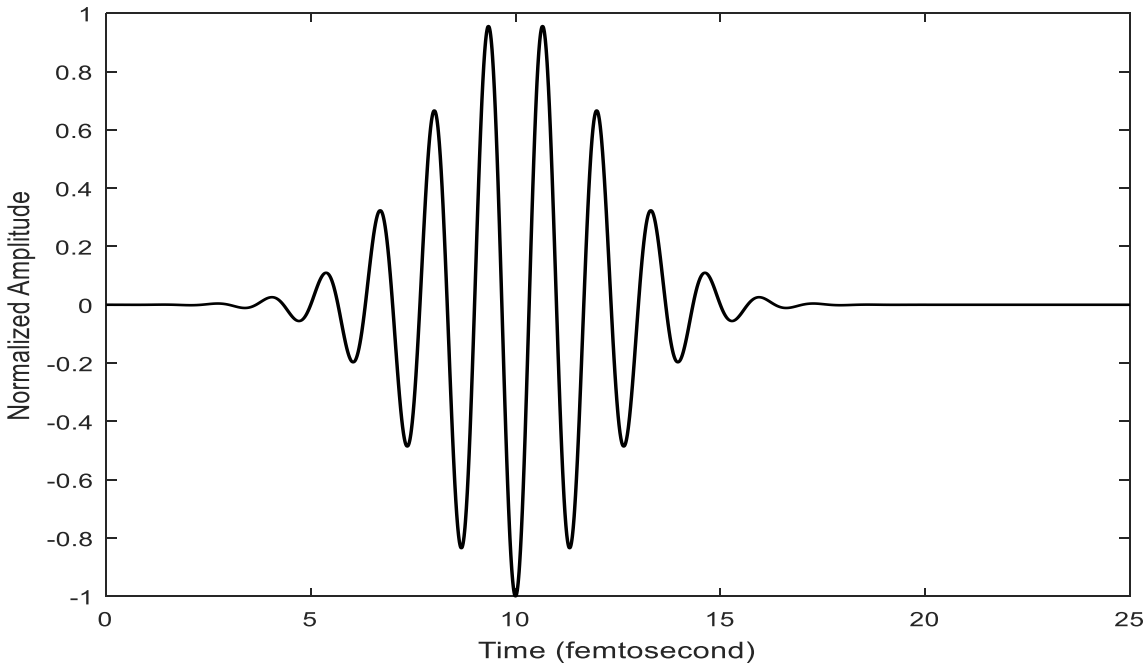

Fig. 6.35: Normalized excitation signal used in the simulation in time domain (Modulated Gaussian pulse with 0.75 PHz cosine wave).

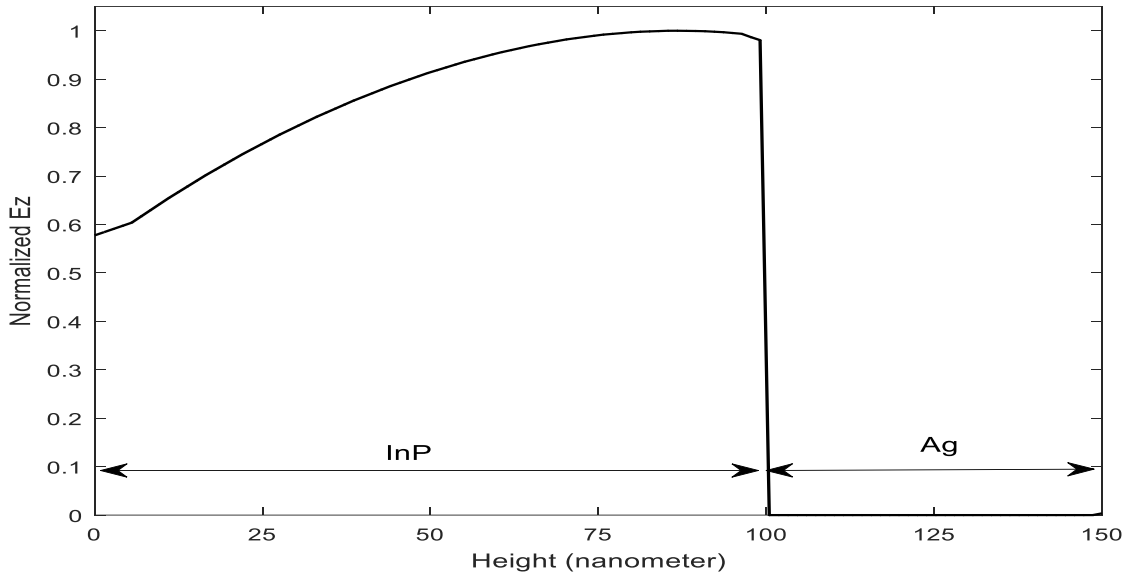

Fig. 6.36: Normalized Ez profile in the material structure.

Gaussian pulse is widely used in particular for high frequency calculation and has been used as the excitation signal for the simulation with frequency ranging from 352.9THz to 1000THz [9].

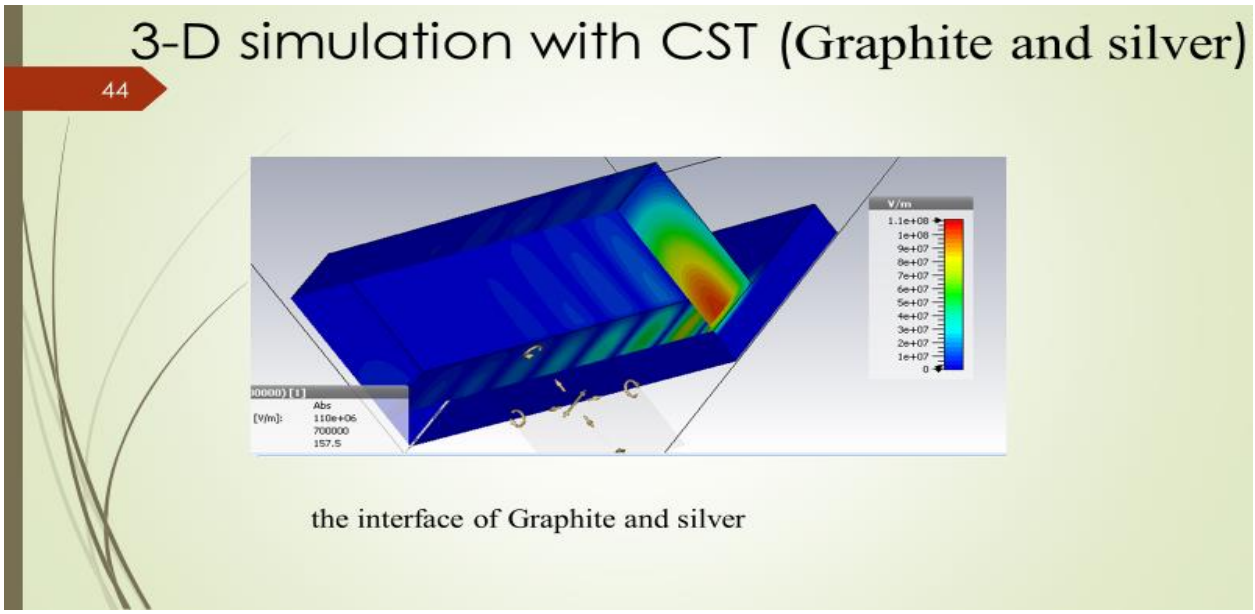

Fig. 6.37: The SSP propagation at the interface of silver and InP.

CHAPTER 7

SIMULATION RESULTS OF SINGLE INTERFACE PLASMONIC STRUCTURE

Propagation characteristics of Surface Plasmon Polaritons (SPPs) in the single interface of Silver (Ag) and Indium Phosphide (InP) are presented here. A three-dimensional structure has been designed to analyze the dynamics of the propagation numerically. Efficiency, voltage standing wave ratio (VSWR), return loss, reflection coefficient are explored in order to analyze the effect of dimension change which has been shown in this chapter.

7.1 SPPs in single interface of Silver (Ag) and Indium Phosphide (InP)

A three-dimensional view of the single interface Ag-InP structure that was used for the simulation is presented in Fig.7-1. Metal-dielectric interface is made by putting a thin silver film on the top of the bulk InP layer. Here a, b and c represent the length, width, and height of the InP layer while p, q and r represent the length, width, and height of the Ag layer respectively.

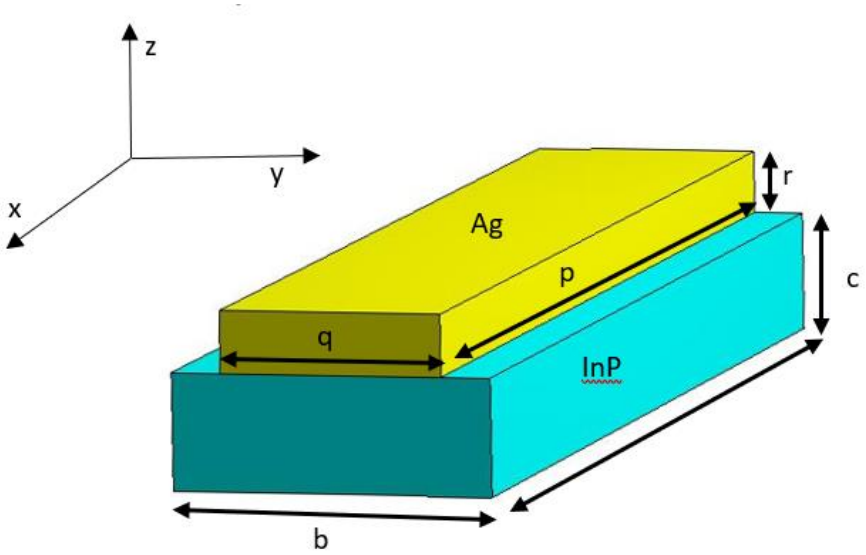

Fig. 7.1: Schematic diagram of the nanoplasmonic structure used for the numerical analysis.

7.2 Input Source

Gaussian pulse is widely used in particular for high frequency calculation and has been used as the excitation signal for the simulation with frequency ranging from 352.9THz to 1000THz [9].

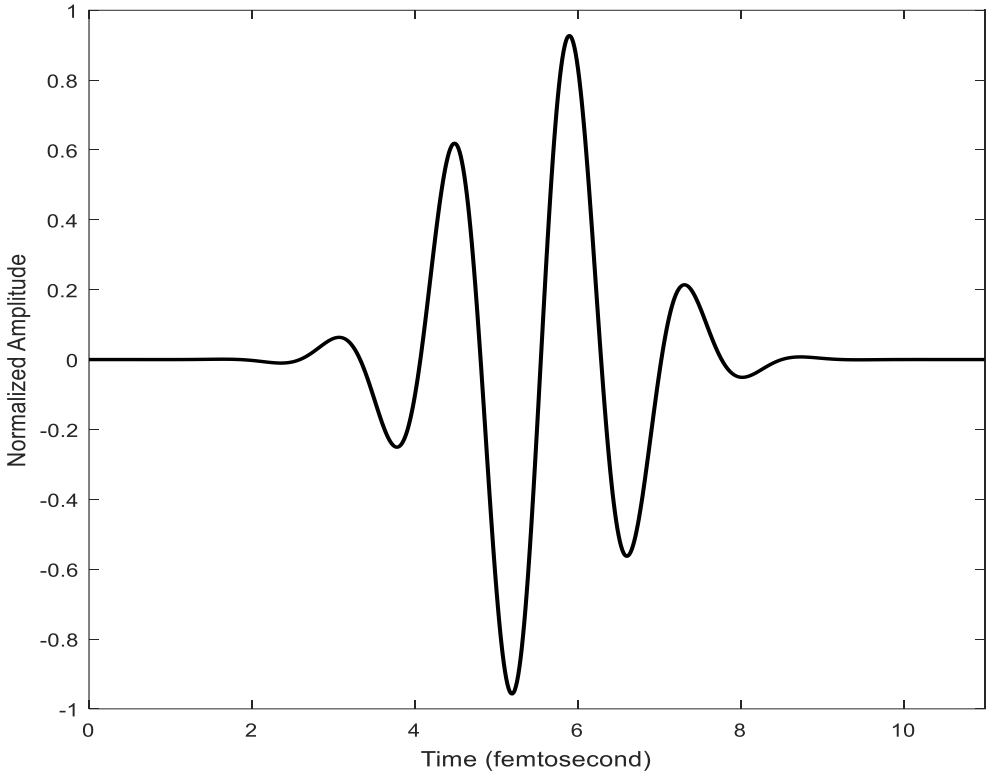

Fig. 7.2: Normalized excitation signal used in the simulation in time domain (Modulated Gaussian pulse with 0.75 PHz cosine wave).

7.3 Ez Profile in Material Structure

Fig. 3 shows that the electric field strength is maximum at the interface of Ag-InP and decreases as one moves away from the interface. But the electric field strength decreases rapidly into the Ag because of heat dissipation.

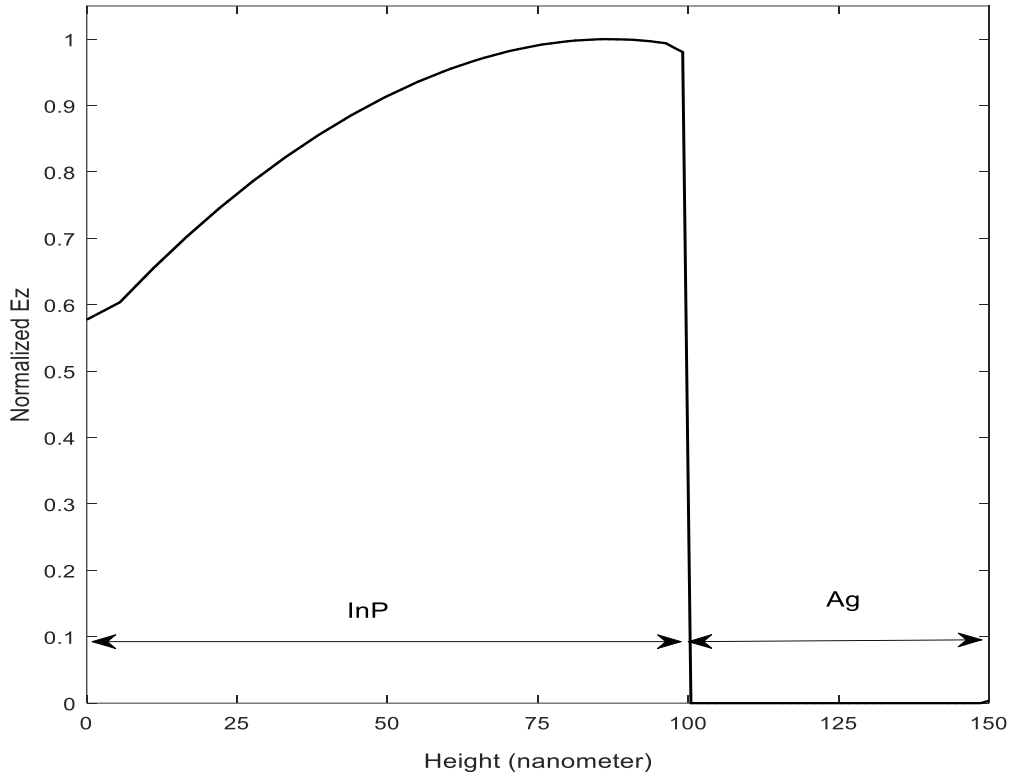

Fig. 7.3: Normalized Ez profile in the material structure.

7.4 Efficiency with different height of InP layer keeping width (b) fixed

The numerically obtained efficiency while varying the height (c) of the InP layer for different input signal wavelengths are shown in fig. 4(i). Here, the length of both InP and Ag is kept fixed at 1000nm (a = p = 1000nm) and width (q) of Ag is taken as 240nm. Although the height of InP is varied from 60nm to 110nm but the width (b) is kept unaltered at 260nm.

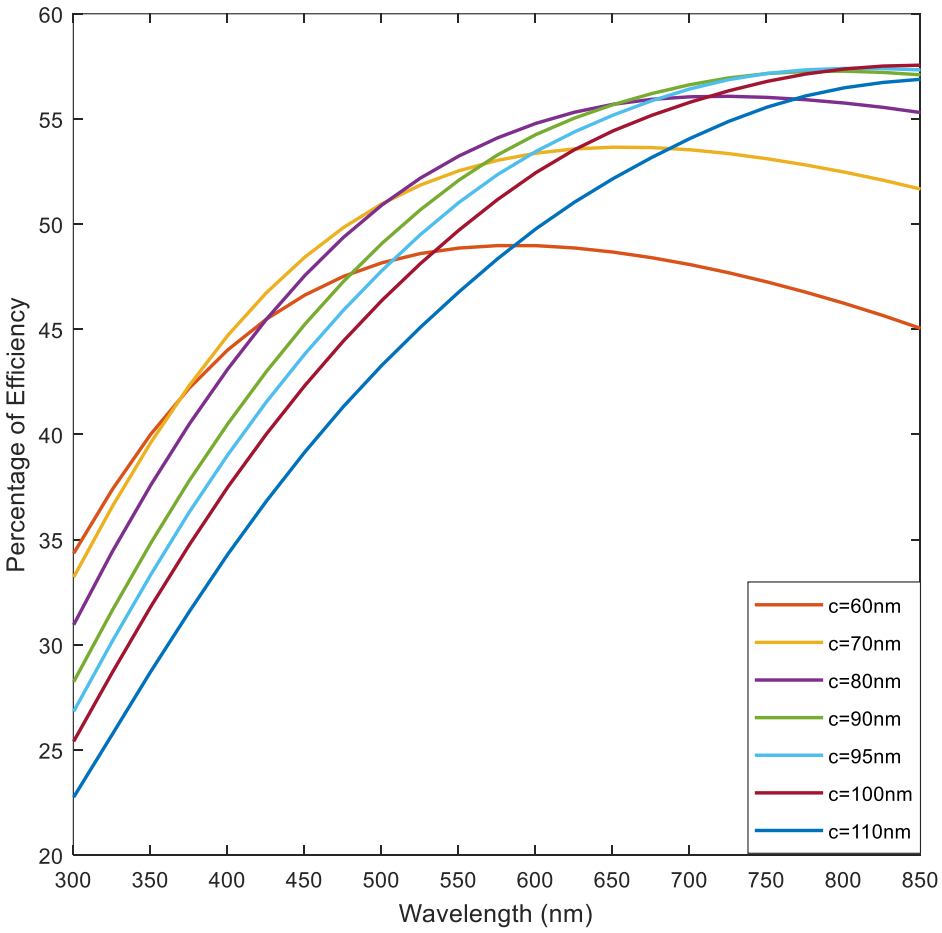

Fig. 7.4: Efficiency as a function of the varying the height of InP layer of the nanoplasmonic structure for the wavelength ranging from 300nm to 850nm.

The variation of efficiency with different height of InP layer has been shown in table I.

TABLE 7.1. Efficiency with different height of InP layer keeping width (b) fixed

Height of InP layer (nm)	**Wavelength at which maximum efficiency occurs (nm)**	**Efficiency**
60	575.40	48.976
70	650.45	53.656
80	725.50	56.076
90	800.55	57.270
95	800.55	57.402
100	850.59	57.556
110	850.59	56.888

7.5 Efficiency with different width of InP Layer keeping height (c) fixed

Since maximum efficiency is found for a structure having the height (c) of 100nm, this height of InP layer is kept fixed while the width (b) of InP is varied. Fig. 4(ii) shows efficiency as the width (b) of InP is varied for a range of input wavelength from 300nm to 850nm. For most of the structures, efficiency escalated as the wavelength is gradually increased reaching the peak for a particular wavelength. InP layer having the width (b) of 355nm gives the highest efficiency.

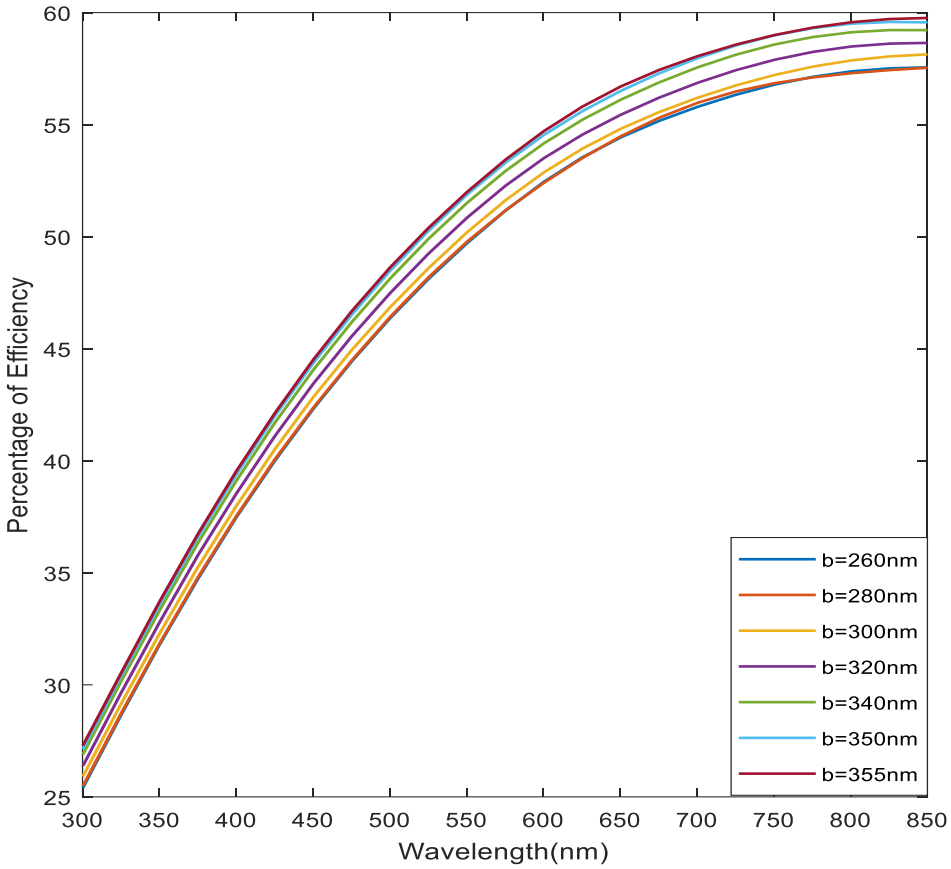

Fig 7.5: Efficiency as a function of the varying the width of InP layer of the nanoplasmonic structure for the wavelength ranging from 300nm to 850nm.

The effect of variation of width (b) on efficiency is also shown in table II.

TABLE 7.2. Efficiency with different width of InP Layer keeping height (c) fixed

Width of InP layer (nm)	**Wavelength at which maximum efficiency occurs (nm)**	**Efficiency**
260	850.59	57.556
280	850.59	57.540
300	850.59	58.136
320	850.59	58.648
340	825.57	59.219
350	825.57	59.582
355	850.59	59.761

7.6 Analysis of the nanoplasmonic structure with the InP layer having a width (b) of 340nm and height (c) of 100nm

Further increase of the width does not increase the efficiency appreciably but makes the circuit bulky. So, the structure with the InP layer having a width (b) of 340nm and height (c) of 100nm is used for further analysis.

The reflection coefficient is measured as a function of wavelength for the wavelength ranging from 300 nm to 850 nm and presented in fig. 5(i). From the figure, it can be observed that the reflection coefficient increases as we increase the input wavelength reaching a maximum value at the input wavelength of 850nm. The maximum value of reflection coefficient is 0.082 which indicates a negligible amount of reflection for the structure.

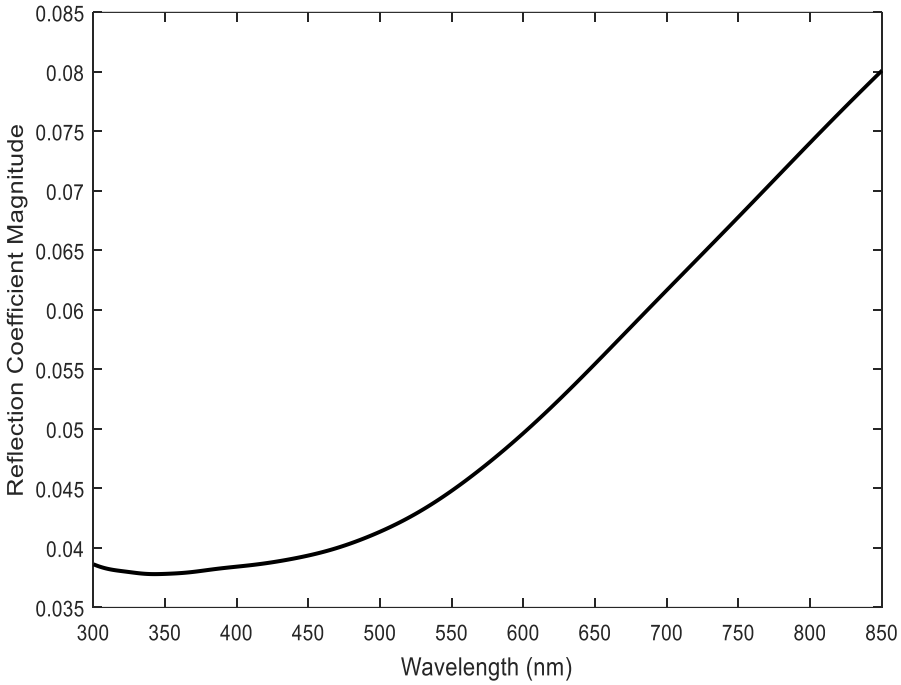
Reflection Coefficient Magnitude
0.085
0.08
0.075
0.07
0.065
0.06
0.055
0.05
0.045
0.04
0.035
300
350
400
450
500
550
600
650
700
750
800
850
Wavelength (nm)

(i)

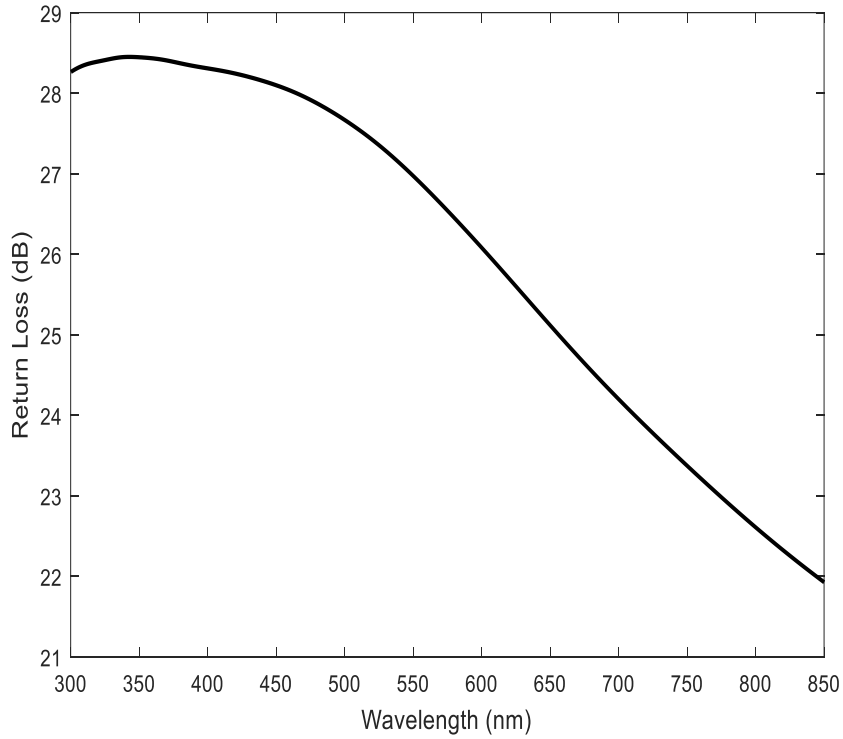
Return Loss (dB)
29
28
27
26
25
24
23
22
21
300
350
400
450
500
550
600
650
700
750
800
850
Wavelength (nm)

(ii)

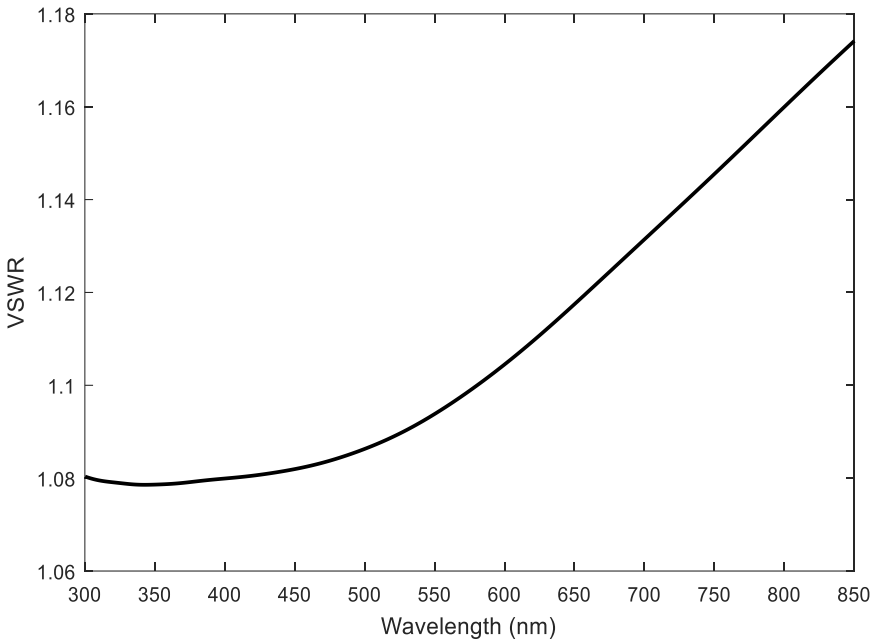

(iii)

Fig. 7.6: (i) Reflection coefficient, (ii) return loss and (iii) voltage standing wave ratio (VSWR) of the nanoplasmonic structure for the wavelength ranging from 300nm to 850nm.

Both the return loss and VSWR are the function of the reflection coefficient and obtained from analytical equations which are shown in fig. 5(ii and iii). Here, the VSWR remains very close to unity for the entire range of wavelengths ensuring efficient power transmission. The value of the VSWR remains almost consistent for the wavelengths from 300nm to 450nm which is 1.08 and then increases almost linearly from 450nm to 850nm. So, it indicates a lower impedance mismatch for our proposed nanoplasmonic structure.

The transmission coefficient obtained from the simulation is shown in fig. 6(i). A decreasing trend of transmission coefficient is found for the wavelengths from 325nm to 700nm after that it remains almost constant at 0.287. The insertion loss is found analytically since it is a function of transmission coefficient and is exhibited in fig. 6(ii).

The electric field distribution in the single interface of Ag-InP has been shown in fig. 7. The strength of the electric field decreases as we move away from the interface of Ag-InP. The electric field decreases exponentially in the positive z direction as we move into the Ag

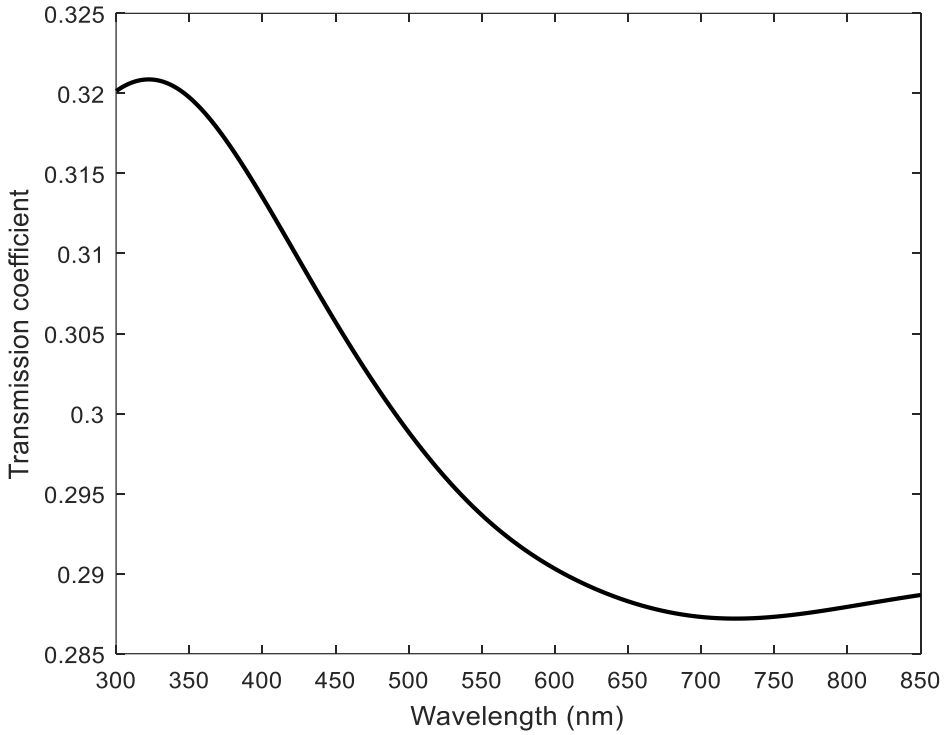

(i)

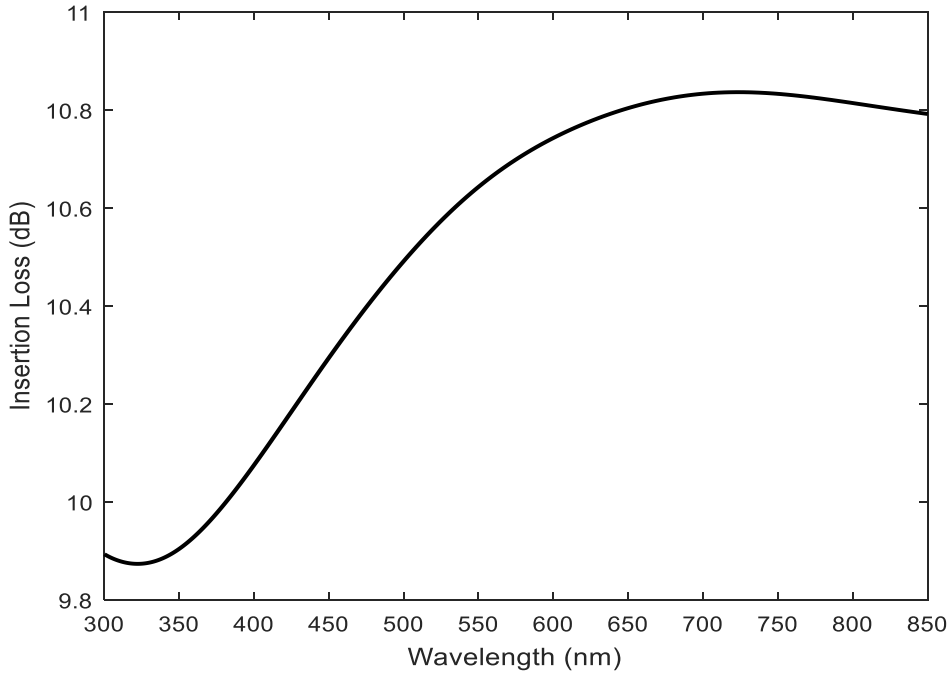

(ii)

Fig. 7.6: (i) Transmission coefficient, (ii) insertion loss of the nanoplasmonic structure for the wavelength ranging from 300nm to 850nm.

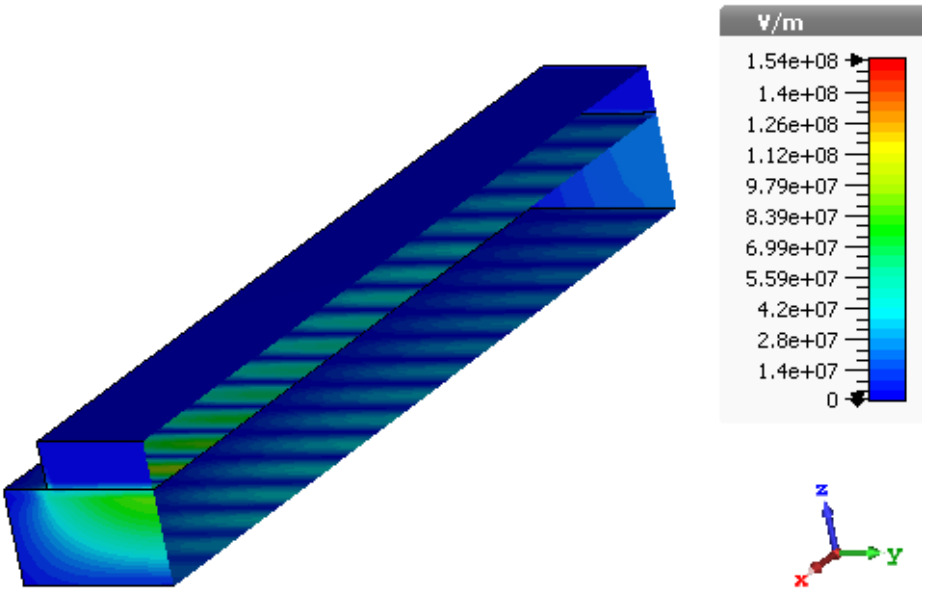

Fig. 7.8: Electric field distribution in the single interface of Ag and InP.

CHAPTER 8

NUMERICAL CONSIDERATION

8.1 Numerical Stability Limit

The velocity of propagation of numerical wave depends on the space increment Δt. Equation 8.1

$$\Delta t \leq \Delta t_{\max} = \frac{1}{c\sqrt{\frac{1}{\Delta x^2}+\frac{1}{\Delta y^2}+\frac{1}{\Delta z^2}}} \quad (8.1)$$

This Stability criterion of the equation (8.1) was derived for a linear system. For nonlinear model like InP, the simulator may sometimes become unstable. So, we reduced the time by 5% below of equation (8.1). So, the step equation becomes

$$\Delta t = \frac{.95}{c\sqrt{\frac{1}{\Delta x^2}+\frac{1}{\Delta y^2}+\frac{1}{\Delta z^2}}} \quad (8.2)$$

8.2 Dimensional Limit

The length of the InP and Ag layers have been kept fixed (a = p = 1000nm) while we vary both height (c) and width (b) of InP layer. Here, we varied the height of the InP layer from 60nm to 110nm and width from 260nm to 355nm. Further increase of the width does not increase the efficiency appreciably but makes the circuit bulky and the time of simulation by great extent.

CHAPTER 9

CONCLUSIONS AND FUTURE WORK

9.1 Summary and Conclusions

- A detailed analysis of SPP propagation through a single interface of InP and Ag has been presented. In the simulation, the frequency dependent dispersion relation has been considered for both Ag and InP.
- The dimensions of the structure have been varied to achieve an efficiency of 59.76%. The structure having the highest efficiency is further used to measure reflection coefficient, return loss, VSWR, transmission coefficient and insertion loss which are essential for understating the performance of SPP propagation.
- In the future, this investigation will be helpful for the design and fabrication process of photonic integrated circuits (PICs).

9.2 Future work

- Propagation Characteristics of InP will help the designer to design a coupler based on InP
- Similar approach can be followed to find the characteristics of SPP propagation in single interface of other metals and dielectrics

References

[1] D.K. Gramotnev, S.I. Bozhevolnyi, Plasmonics beyond the diffraction limit, Nat. Photonics 4 (2010) 83–91.
[2] D. O. Melville, R. J. Blaikie, and C. Wolf, "Super-resolution imaging through a planar silver layer," Opt. Express, vol. 13,no. 6,pp. 2127-2134,2005.
[3] J. Rho, Z. Ye, Y. Xiong, X. Yin, Z. Liu, H. Choi, G. Bartai, and X. Zhang, "Spherical hyperlens for two-dimensional sub-diffractional imaging at visible frequencies," Nature communications, vol. 1,p. 143,2010.
[4] C. Jung, S. Yee, K. Kuhn, Integrated optics waveguide modulator based on surface plasmon resonance, J. Light. Technol. 12 (1994) 1802–1806.
[5] T. Nikolajsen, K. Leosson, S.I. Bozhevolnyi, Surface plasmon polariton based modulators and switches operating at telecom wavelengths, Appl. Phys. Lett. 85 (2004) 5833–5835.
[6] A. Hosseini, Y. Massoud, A low-loss metal–insulator–metal plasmonic Bragg reflector, Opt. Express 14 (2006) 11318–11323.
[7] Y. Shen, T. Lo, P. Taday, B. Cole, W. Tribe, M. Kemp, Detection and identification of explosives using terahertz pulsed spectroscopic imaging, Appl. Phys. Lett. 86 (2005) 241116.
[8] M. Nagel, M. Forst, H. Kurz, "THz biosensing devices: fundamentals and technology", J. Phys. Condens. Matter 18 (2006) S601.
[9] M. G. Saber, R. H. Sagor, "Design and analysis of a gallium lanthanum sulfide based nanoplasmonic coupler yielding 67% efficiency," vol. 125, no. 18, pp. 5374-5377, 2014.
[10] Lou, Fei, et al. "Experimental demonstration of ultra-compact directional couplers based on silicon hybrid plasmonic waveguides." *Applied Physics Letters* 100.24 (2012): 241105.
[11] K. Yee, "Numerical solution of initial boundary value problems involving Maxwell's equations in isotropic media," Antennas and Propagation, IEEE Transactions on, vol. 14, pp. 302-307, 1966.
[12] Gururaj V. Naik, Jongbum Kim, and Alexandra Boltasseva, "Oxides and nitrides as alternative plasmonic materials in the optical range [Invited]," Opt. Mater. Express **1**, 1090-1099 (2011)
[13] M. E. Aryaee Panah, O. Takayama, S. V. Morozov, K. E. Kudryavtsev, E. S. Semenova, and A. V. Lavrinenko, "Highly doped InP as a low loss plasmonic material for mid-IR region," Opt. Express **24**, 29077-29088 (2016)
[14] A. Taflove and S. C. Hagness, "Computational Electrodynamics: The Finite-Difference Time-Domain Method (Artech House, Boston, 2000)," pp. 273-328, 2001.
[15] R. H. Sagor, K. A. Shahriar, M. G. Saber, M. M. A. Joy, and I. H. Sohel, "Modeling of Dispersive Materials Using Dispersion Models for FDTD Application," vol. 8, no. 2, pp. 251-275, 2016.
[16] A. V. Deinega, I. V. Konistyapina, M. V. Bogdanova, I. A. Valuev, Yu. E. Lozovik, and B. V. Potapkin, "Optimization of an anti-reflective layer of solar panels based on ab initio calculations," vol. 52, no. 11, pp. 1128-1134, 2009.
[17] A. D. Rakić, A. B. Djurišić, J. M. Elazar, and M. L. Majewski, "Optical properties of metallic films for vertical-cavity optoelectronic devices," vol. 37, no. 22, pp. 5271-5283, 1998